AD-A037 688 NAVAL AIR DEVELOPMENT CENTER WARMINSTER PA AIR VEHICL--ETC F/G 20/4
LOW-SPEED V/STOL STABILITY AND CONTROL PREDICTION. VOLUME I. MO--ETC(U)
JAN 77 J W CLARK

UNCLASSIFIED NADC-76312-30 NL

1 OF 1
AD A037688

END
DATE FILMED
4-77

REPORT NO. NADC-76312-30

12 B.S.

LOW-SPEED V/STOL STABILITY AND CONTROL PREDICTION - VOLUME I: MODEL DESCRIPTION AND VALIDATION

J. W. Clark, Jr.
Air Vehicle Technology Department
NAVAL AIR DEVELOPMENT CENTER
Warminster, Pennsylvania 18974

11 JANUARY 1977

INTERIM REPORT
AIRTASK NO. A03V-320D/001B/6F41421201

APPROVED FOR PUBLIC RELEASE; DISTRIBUTION UNLIMITED

Prepared for
NAVAL AIR SYSTEMS COMMAND
Department of the Navy
Washington, D.C. 20361

NOTICES

REPORT NUMBERING SYSTEM - The numbering of technical project reports issued by the Naval Air Development Center is arranged for specific identification purposes. Each number consists of the Center acronym, the calendar year in which the number was assigned, the sequence number of the report within the specific calendar year, and the official 2-digit correspondence code of the Command Office or the Functional Department responsible for the report. For example: Report No. NADC-76015-40 indicates the fifteenth Center report for the year 1976, and prepared by the Crew Systems Department. The numerical codes are as follows:

CODE	OFFICE OR DEPARTMENT
00	Commander, Naval Air Development Center
01	Technical Director, Naval Air Development Center
02	Program and Financial Management Department
09	Technology Management Office
10	Naval Air Facility, Warminster
20	Aero Electronic Technology Department
30	Air Vehicle Technology Department
40	Crew Systems Department
50	Systems Department
60	Naval Navigation Laboratory
81	Technical Support Department
85	Computer Department

PRODUCT ENDORSEMENT - The discussion or instructions concerning commercial products herein do not constitute an endorsement by the Government nor do they convey or imply the license or right to use such products.

APPROVED BY: _____ DATE: 11 January 1976

P. M. STURM
Commander, USN
Deputy Director, AVTD

UNCLASSIFIED

SECURITY CLASSIFICATION OF THIS PAGE (When Data Entered)

REPORT DOCUMENTATION PAGE

READ INSTRUCTIONS BEFORE COMPLETING FORM

1. REPORT NUMBER: NADC-76312-30	2. GOVT ACCESSION NO.
3. RECIPIENT'S CATALOG NUMBER	
4. TITLE (and Subtitle): LOW-SPEED V/STOL STABILITY AND CONTROL PREDICTION • VOLUME I: MODEL DESCRIPTION AND VALIDATION •	5. TYPE OF REPORT & PERIOD COVERED: INTERIM REPORT. •
	6. PERFORMING ORG. REPORT NUMBER
7. AUTHOR(s): J. W. CLARK, JR.	8. CONTRACT OR GRANT NUMBER(s)
9. PERFORMING ORGANIZATION NAME AND ADDRESS: AIR VEHICLE TECHNOLOGY DEPARTMENT (CODE 30) NAVAL AIR DEVELOPMENT CENTER WARMINSTER, PA. 18974	10. PROGRAM ELEMENT, PROJECT, TASK AREA & WORK UNIT NUMBERS: AIRTASK NO. A03V-320D/001B/ 6F41421201
11. CONTROLLING OFFICE NAME AND ADDRESS: NAVAL AIR SYSTEMS COMMAND DEPARTMENT OF THE NAVY WASHINGTON, D. C. 20361	12. REPORT DATE: 11 Jan[illegible]77
	13. NUMBER OF PAGES: 85
14. MONITORING AGENCY NAME & ADDRESS(if different from Controlling Office): 89p.	15. SECURITY CLASS. (of this report): UNCLASSIFIED
	15a. DECLASSIFICATION/DOWNGRADING SCHEDULE

16. DISTRIBUTION STATEMENT (of this Report)

Approved for public release; distribution unlimited.

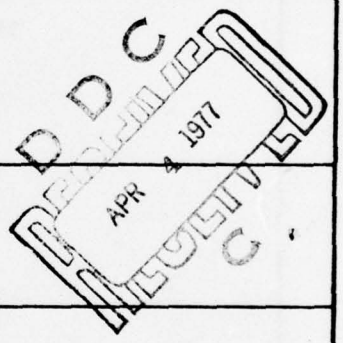

17. DISTRIBUTION STATEMENT (of the abstract entered in Block 20, if different from Report)

18. SUPPLEMENTARY NOTES

19. KEY WORDS (Continue on reverse side if necessary and identify by block number)

Stability and Control
Flying Qualities
V/STOL Aircraft
V/STOL Aerodynamics

20. ABSTRACT (Continue on reverse side if necessary and identify by block number)

A unified prediction method is developed to support V/STOL Stability and Control analyses. The method is geared to a preliminary design environment to facilitate its application using the limited type of data normally available early in the design process. Volume I describes the models which were developed or modified and their validation. Volume II describes the computer program incorporating these models and the associated input data requirements and output format.

DD FORM 1 JAN 73 1473 EDITION OF 1 NOV 65 IS OBSOLETE S/N 0102-014-6601 |

UNCLASSIFIED

SECURITY CLASSIFICATION OF THIS PAGE (When Data Entered)

407207

SUMMARY

A unified prediction method has been developed to support V/STOL Stability and Control analyses. The method is geared to a preliminary design environment to facilitate its application using the limited data which are normally available early in the aircraft design process.

Mathematical models have been formulated for the force and moment contributions of each of the vehicle components and then combined to allow for prediction of: non-linear, six DOF (Degrees of Freedom) trim conditions; three DOF, small perturbation stability characteristics; six DOF response time histories for arbitrary control and disturbance inputs. The structure of the methodology follows, in a gross sense, a similar methodology for helicopter and stoppable rotor aircraft (reference (a)), with considerable modification of the individual component models. Primary emphasis has been placed on the jet lift and lift/cruise fan classes of V/STOL vehicles in the hover and transition flight regimes but the methods should be easily extendable to include other classes of vehicles.

The methods have been programmed for the CDC 6600 computer and have been validated, with reasonable success, using available XV-6A Kestrel and AV-8A Harrier static and dynamic data. Results of the validation effort are presented in Appendix A.

Documentation is in two volumes. This volume, Volume I, describes the component models, analytical methods and validation results. Volume II constitutes a User Manual for the digital computer program.

TABLE OF CONTENTS

LIST OF FIGURES

LIST OF TABLES

I N T R O D U C T I O N

The stability and control characteristics of V/STOL aircraft in hover and transition flight can be quite different than those of CTOL aircraft in the corresponding take-off and power approach flight regimes. V/STOL aircraft are usually unstable at low speeds and experience propulsion induced aerodynamic and inlet momentum drag effects which are normally neglected for CTOL aircraft. The problem is further complicated by additional control functions such as primary engine nozzle angle and differential thrust and RCS (Reaction Control System) thrust modulation. A recent survey of V/STOL aircraft designers (reference (b)) has indicated a serious need for V/STOL stability and control prediction methods to support preliminary design, configuration trade-offs and evaluations. To this end, the development described herein was undertaken.

Many past efforts in this field have been limited to uncoupled, two or three DOF analyses at small angles of attack and sideslip. Since V/STOL vehicles may exhibit significant cross-coupling between longitudinal and lateral axes, it is necessary to consider full six DOF simulation with cross-axis coupling. Angles of attack and sideslip from 0° to $\pm$180° may be encountered in low-speed flight requiring complete non-linear aerodynamic modelling. Additionally, provision must be made for adequate modelling of aerodynamic interference effects resulting from propulsion system efflux interaction with the surrounding vehicle surfaces. All of the above effects and other less significant ones were included in the model formulation. Figure 1 summarizes the major model components.

The prediction technique has been developed primarily for application in a preliminary design environment and, hence, does not require extensive wind tunnel or propulsion system data tables. This, of course, has some impact on the accuracy of the results but validation with flight test data for an existing vehicle (XV-6A Kestrel) has exhibited an adequate degree of accuracy for preliminary vehicle design, configuration trade-off and design evaluation from a stability and control viewpoint. The methodology, in its current status, is applicable to lift plus lift/cruise and lift/cruise turbojet and fan configurations. However, the general model structure is such that extension to include additional vehicle classes is certainly feasible.

The aerodynamic model of the airframe is divided into four major sections: fuselage, wing, horizontal tail (conventional aft tail or canard) and vertical tail. Each component is modelled separately using a combination of theoretical computations and empirical curve fits over the complete angle of attack and sideslip range. Aerodynamic effects which are not directly related to one of these sections (e.g., landing gear effects) are included in the fuselage simulation for simplicity. Propulsion induced aerodynamic interference effects are accounted for by using curve fits of estimated and available experimental data.

A maximum of two fixed jet nozzles and six vectorable jet nozzles may be simulated, with control being maintained over the thrust of all jets and nozzle angles. In addition to the main jet nozzles, a maximum of ten RCS nozzles and their associated control functions may also be simulated.

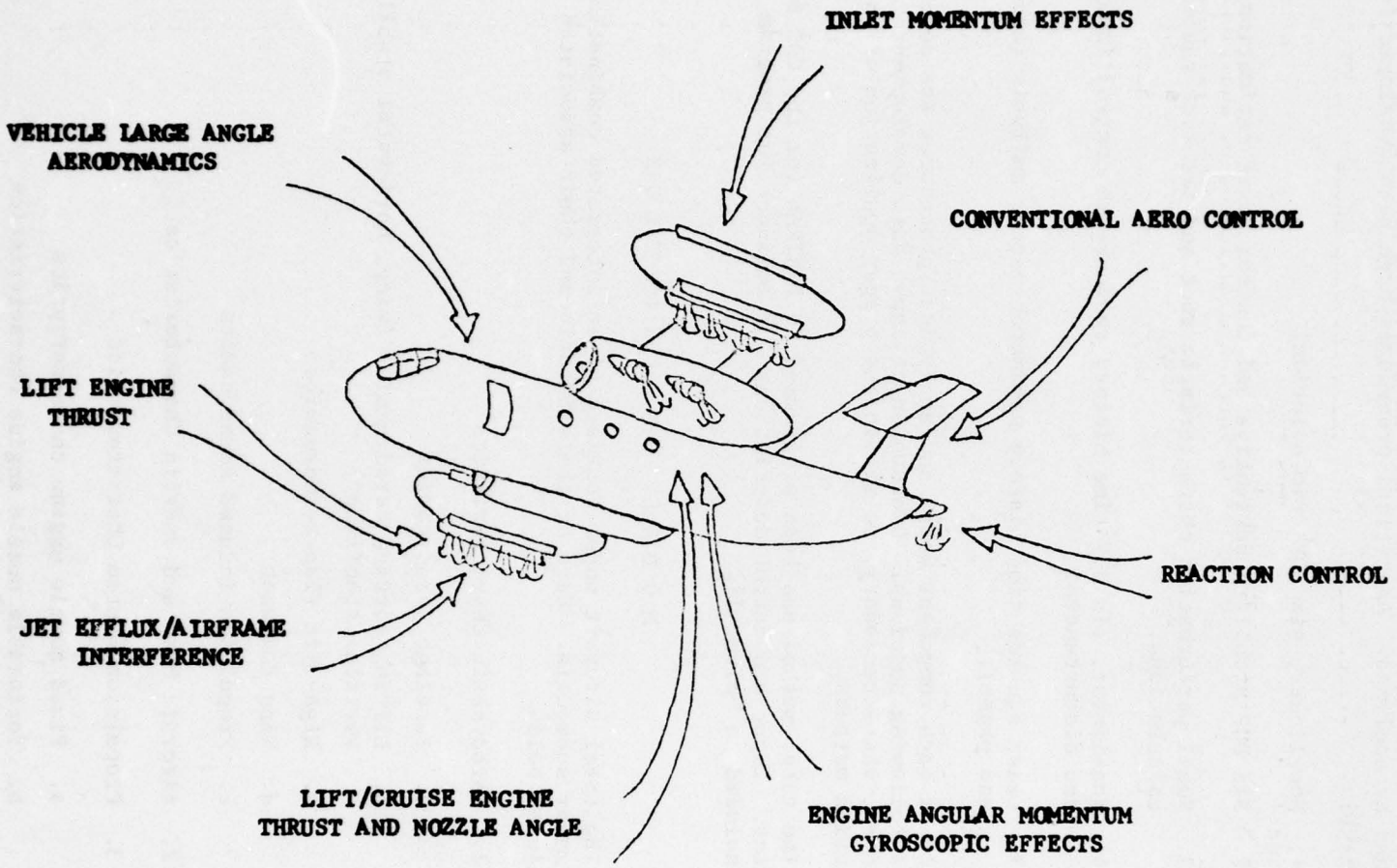

NADC-76312-30

FIGURE 1: VEHICLE MODEL COMPONENTS

All component models are combined to form the total vehicle model which may then be analyzed. Analytical procedures have been developed for the following:

1. Non-linear, six DOF trim solution;
2. Six DOF stability derivative and control power estimation;
3. Small perturbation characteristic root and transfer function calculations;
4. Non-linear, six DOF time history response to control inputs and disturbances;
5. Least squares time history parameter vector analysis (amplitude and phase).

Details of each component model and analytical procedures are described in the following sections. Discussion of input data development is presented, where necessary, to aid in the proper application of the prediction methods.

The total method has been programmed in FORTRAN for the CDC 6600 computer. Input and output descriptions and guidance for program application are included in Volume II.

M O D E L D E S C R I P T I O N

The total aircraft model consists of an integrated combination of four major submodels. Each of the submodels and their associated components are listed below.

1. Aerodynamic Characteristics
   a. Fuselage aerodynamics
   b. Lifting surface aerodynamics (wing, horizontal stabilizer, vertical stabilizer)
   c. High-lift flap aerodynamics
   d. Wing downwash
   e. Propulsion-induced aerodynamics
2. Aircraft Mass and Inertia Characteristics
3. Propulsion System Characteristics
   a. Fixed nozzle engine characteristics
   b. Vectorable nozzle engine characteristics
   c. Inlet momentum effects
   d. Angular momentum effects

4. Control System Characteristics

   a. Aerodynamic control surfaces

   b. Reaction control nozzle characteristics

   c. Thrust management control characteristics (magnitude and direction)

Forces and moments produced by each component are calculated in a localized axis system and then resolved to a fixed set of reference aircraft body axes with the X-axis directed forward, Y-axis directed toward the right wing tip and Z-axis directed down. The centers of action of each component force and moment system are located in the aircraft reference system by FS (Fuselage Station) increasing in the negative X direction, BL (Butt Line) increasing in the positive Y direction and WL (Water Line) increasing in the negative Z direction. Each component force and moment system is transferred to the aircraft center of gravity and all are summed to yield the total force and moment acting on the vehicle.

Each component model will now be described in detail.

AERODYNAMIC CHARACTERISTICS

Fuselage Aerodynamics

Aerodynamic characteristics of the fuselage are modelled in a body axis frame of reference as axial, side and normal force; pitch and yaw moments. Roll moment is not an explicit model input but evolves from applying side force through the vertical moment arm between the fuselage aerodynamic reference center and the vehicle center of gravity. Figure 2 shows the orientation and sign convention of the fuselage forces and moments.

Since one of the objectives of the prediction method is to simulate vehicle characteristics throughout hover and transition, force and moment models for the complete angle of attack (α) and sideslip (α_y) range are required. In the case of the fuselage, it is assumed to be sufficient to concentrate on the 0 to +180 degree range with the following assumptions applied to account for the 0 to -180 degree range.

$$A(-\alpha) = A(\alpha) \tag{1a}$$

$$S(-\alpha_y) = -S(\alpha_y) \tag{1b}$$

$$N_f(-\alpha) = -N_f(\alpha+2\alpha_o) \tag{1c}$$

$$M(-\alpha) = -M(\alpha+2\alpha_o) \tag{1d}$$

$$N(-\alpha_y) = -N(\alpha_y) \tag{1e}$$

Inherent in equations (1) are the assumptions that side force, S, and yaw moment, N, are zero at $\alpha_y = 0$, axial force, A, has a minimum at $\alpha = \alpha_y = 0$,

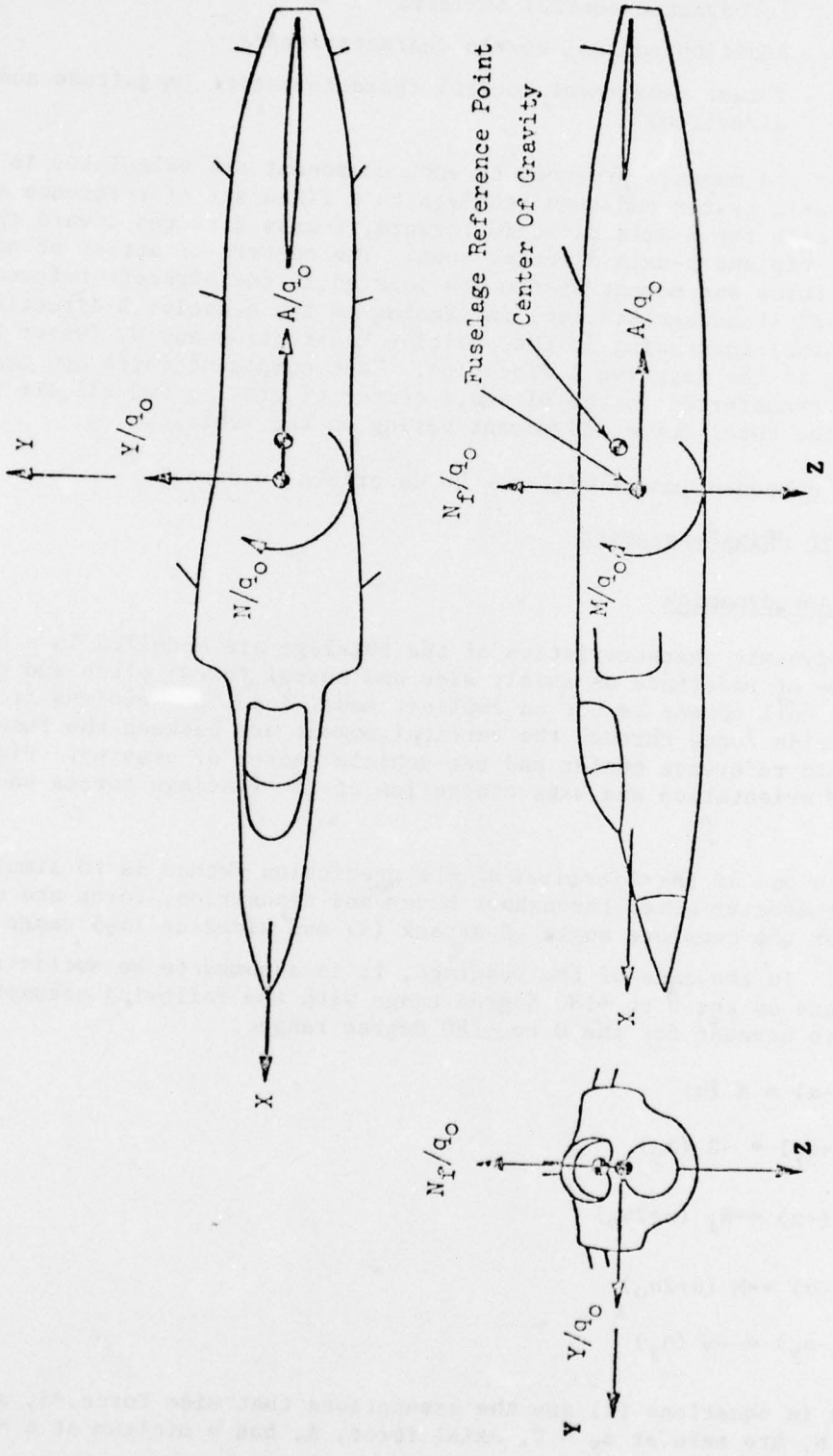

FIGURE 2: FUSELAGE FORCE AND MOMENT CONVENTIONS

and normal force, N_f, and pitch moment, M, are zero at $\alpha = \alpha_o$. The aerodynamic angles α and α_y are defined by:

$$\alpha = \tan^{-1} (w/u) \tag{2a}$$

$$\alpha_y = \tan^{-1} (v/u) \tag{2b}$$

where u, v, and w are the body axis velocities in the X, Y, and Z directions, respectively.

The aerodynamic forces and moments of the fuselage must be determined from experimental data or estimated by theoretical or semi-empirical means. Reference (c) describes a very convenient digital computer technique for estimating the aerodynamic characteristics of symmetrical bodies over the entire angle range. It also includes a very good bibliography of other currently available techniques. Figure 3 presents the results of applying the method of reference (c) to the XV-6A (Kestrel) fuselage. These data were used during validation which is described in a later section. The data are normalized by dynamic pressure, q_o, to allow for varying flight velocities.

The data curves of Figure 3 are typical of fuselage aerodynamics and may be reasonably approximated by the equations presented in Table I. Though the equations may seem somewhat complex, a closer inspection reveals that determining the required coefficients is really quite simple. $(A/q_o)_o$ is the value of the axial force at zero angle of attack. $(\ )_{max}$ is the maximum value of the corresponding force between 0 and 180 degrees. $(\ )_{max_1}$ and $(\ )_{max_2}$ are the maximum values of the corresponding moment between 0 and 90 degrees and 90 and 180 degrees, respectively. Note that $(M/q_o)_{max_2}$ and $(N/q_o)_{max_2}$ are usually negative. The moments take on zero value at some angle between 0 and 180 degrees; these angles are denoted by α_1 for pitch and α_2 for yaw. Once the preceeding coefficients are determined, the various exponents, n_i, may be calculated by substituting a force or moment value for an angle in the range which is to be most accurately approximated and solving for the exponent. The moment coefficients are assumed to be linear over a $\pm 10°$ range about zero to preclude problems with the infinite slope characteristic of $(\sin x)^n$ at the origin for $n < 1$. Figure 3 presents one possible approximation to the XV-6A data. The corresponding functional expressions are included in Table II.

Using the functions of Table I, the fuselage force and moment coefficients are calculated for a specific α and α_y. They must then be dimensionalized, resolved into the proper body axes and transferred to the vehicle CG.

The coefficients are dimensionalized using the component of dynamic pressure in the coordinate plane corresponding to that of the coefficient. That is:

$$A = q_o \, (A/q_o(\alpha_t))$$

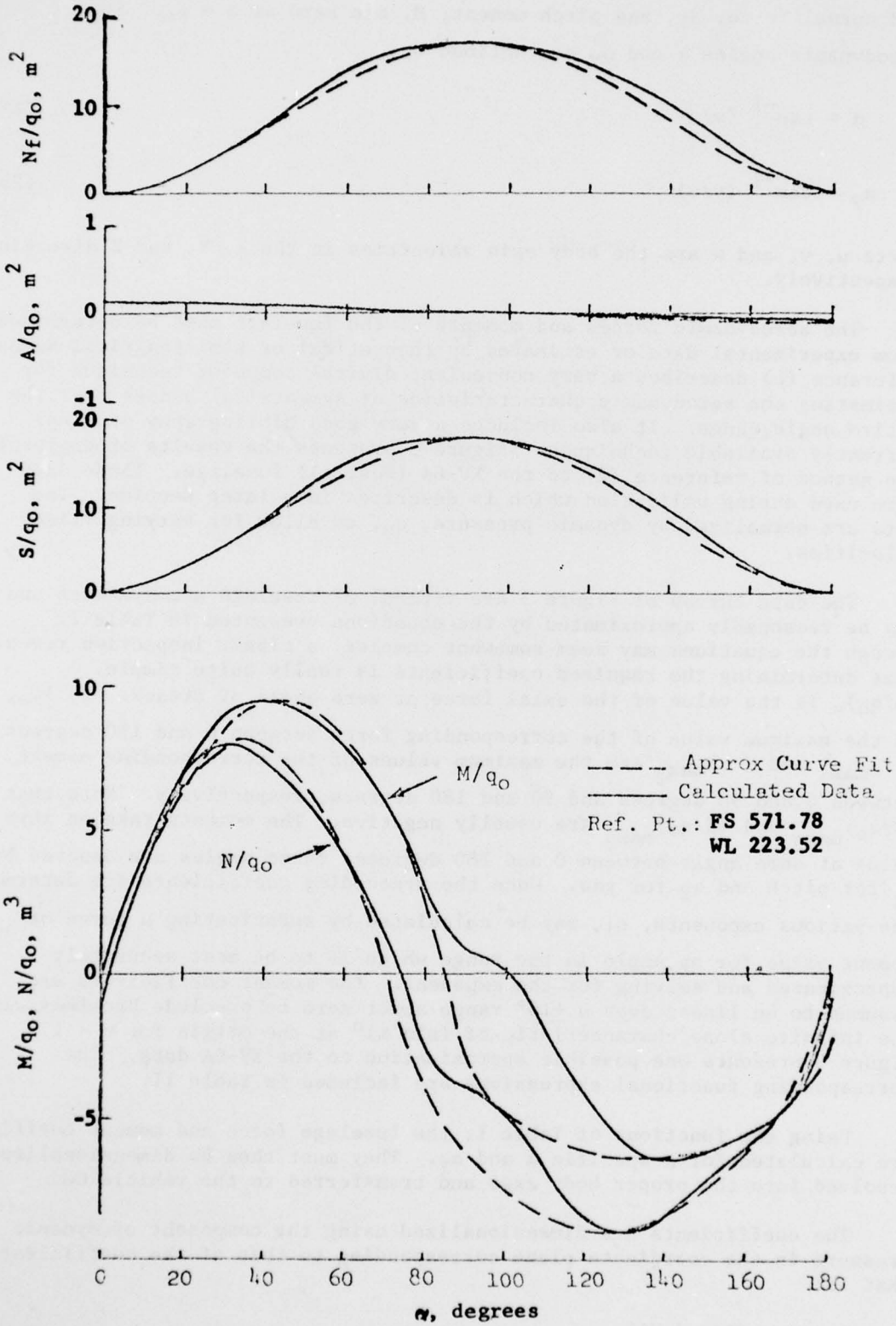

FIGURE 3: XV-6A FUSELAGE AERODYNAMICS

TABLE I

Approximate Fuselage Aerodynamic Functions

$$A/q_o(\alpha) = (A/q_o)_o \, \text{sign}(\cos\alpha) \left|\cos\alpha\right|^{n_1}$$

$$S/q_o(\alpha_y) = (S/q_o)_{max} \, \text{sign}(\sin\alpha_y) \left|\sin\alpha_y\right|^{n_2}$$

$$N_f/q_o(\alpha) = (N_f/q_o)_{max} \, \text{sign}(\sin(\alpha - \alpha_o)) \left|\sin(\alpha - \alpha_o)\right|^{n_3}$$

$$M/q_o(\alpha) = \left[\frac{(M/q_o)\big|_{(\alpha=10^\circ+\alpha_o)} - (M/q_o)\big|_{(\alpha=-10^\circ+\alpha_o)}}{20^\circ}\right](\alpha - \alpha_o) \qquad -10^\circ+\alpha_o < \alpha < 10^\circ+\alpha_o$$

$$M/q_o(\alpha) = (M/q_o)_{max_1}\left[\text{sign}\left(\sin\frac{180^\circ(\alpha - \alpha_o)}{(\alpha_1 - \alpha_o)}\right)\right]\left|\sin\frac{180^\circ(\alpha - \alpha_o)}{(\alpha_1 - \alpha_o)}\right|^{n_4} \qquad \begin{matrix} 2\alpha_o - \alpha_1 \le \alpha \le -10^\circ+\alpha_o \\ 10^\circ+\alpha_o \le \alpha \le \alpha_1 \end{matrix}$$

$$M/q_o(\alpha) = (M/q_o)_{max_2}\left[\text{sign}\left(\sin\frac{180^\circ(\alpha - \alpha_1)}{(180^\circ + \alpha_o - \alpha_1)}\right)\right]\left|\sin\frac{180^\circ(\alpha - \alpha_1)}{(180^\circ + \alpha_o - \alpha_1)}\right|^{n_5} \qquad \begin{matrix} -180^\circ \le \alpha \le 2\alpha_o - \alpha_1 \\ \alpha_1 \le \alpha \le 180^\circ \end{matrix}$$

$$N/q_o(\alpha_y) = \left[\frac{(N/q_o)\big|_{(\alpha_y=10^\circ)} - (N/q_o)\big|_{(\alpha_y=-10^\circ)}}{20^\circ}\right]\alpha_y \qquad -10^\circ < \alpha_y < 10^\circ$$

$$N/q_o(\alpha_y) = (N/q_o)_{max_1}\left[\text{sign}\left(\sin\frac{180^\circ\alpha_y}{\alpha_2}\right)\right]\left|\sin\frac{180^\circ\alpha_y}{\alpha_2}\right|^{n_6} \qquad \begin{matrix} -\alpha_2 \le \alpha_y \le -10^\circ \\ 10^\circ \le \alpha_y \le \alpha_2 \end{matrix}$$

$$N/q_o(\alpha_y) = (N/q_o)_{max_2}\left[\text{sign}\left(\sin\frac{180^\circ(\alpha_y - \alpha_2)}{(180^\circ - \alpha_2)}\right)\right]\left|\sin\frac{180^\circ(\alpha_y - \alpha_2)}{(180^\circ - \alpha_2)}\right|^{n_7} \qquad \begin{matrix} -180^\circ \le \alpha_y \le \alpha_2 \\ \alpha_2 \le \alpha_y \le 180^\circ \end{matrix}$$

TABLE II

XV-6A Fuselage Aero Approximation

$$A/q_o = 0.123 \left| \cos \alpha \right|^{1.8519}$$

$$S/q_o = 17.89 \left| \sin \alpha_y \right|^{1.7676}$$

$$N_f/q_o = 17.12 \left| \sin (\alpha-2) \right|^{1.7583}$$

$$M/q_o = \begin{cases} 9.585 \left| \sin \dfrac{180(\alpha-2)}{83} \right|^{0.8046} & -81 \leq \alpha \leq 85 \\ -6.533 \left| \sin \dfrac{180(\alpha-85)}{97} \right|^{0.3468} & \alpha < -81 \ ; \ \alpha > 85 \end{cases}$$

$$N/q_o = \begin{cases} 8.104 \left| \sin \dfrac{180\alpha}{70} y \right|^{0.7983} & -70 \leq \alpha_y \leq 70 \\ -9.099 \left| \sin \dfrac{180(\alpha_y -70)}{110} \right|^{0.6081} & \alpha_y < -70 \ ; \ \alpha_y > 70 \end{cases}$$

$$S = q_{xy}\ (S/q_o(\alpha_y)) \qquad M = q_{xz}\ (M/q_o(\alpha))$$

$$N_f = q_{xz}\ (N_f/q_o(\alpha)) \qquad N = q_{xy}\ (N/q_o(\alpha_y)) \tag{3}$$

where:

$$\alpha_t = \tan^{-1}\ ((v^2 + w^2)^{1/2}\ /\ u)$$

$$q_{xy} = 1/2\ \rho\ (u^2 + v^2)$$

$$q_o = 1/2\ \rho\ (u^2 + v^2 + w^2)$$

$$q_{xz} = 1/2\ \rho\ (u^2 + w^2) \tag{4}$$

The forces and moments acting in the body axis directions at the fuselage aerodynamic reference point are given by:

$$X_F = -A \qquad L_F = 0$$

$$Y_F = S \qquad M_F = M$$

$$Z_F = -N_f \qquad N_F = N \tag{5}$$

Finally, after transferring to the vehicle CG:

$$\Delta X_F = X_F \qquad \Delta L_F = Z_F(BL_F - BL_{CG}) - Y_F(WL_{CG} - WL_F)$$

$$\Delta Y_F = Y_F \qquad \Delta M_F = M_F + X_F(WL_{CG} - WL_F) - Z_F(FS_{CG} - FS_F)$$

$$\Delta Z_F = Z_F \qquad \Delta N_F = N_F + Y_F(FS_{CG} - FS_F) - X_F(BL_F - BL_{CG}) \tag{6}$$

Lifting Surface Aerodynamics

Basic lift and drag characteristics of the three primary lifting surfaces (wing, horizontal stabilizer and vertical stabilizer) are calculated as functions of angle of attack. The approach used applies to all three and is presented generally. Particular effects which are unique to only one lifting surface are presented following the general discussion. Lift and drag coefficients, C_L and C_D are calculated over the entire angle of attack range from -180 to +180 degrees using primarily geometric data with some basic aerodynamic data estimated based on the methods of references (d) through (f) or similar sources. The calculated forces are assumed to act at the CP (Center of Pressure) of the lifting surface in directions parallel and perpendicular to the local velocity (V_1) which is deflected from the

freestream velocity (V) by the induced angle of attack, α_i. Figure 4 describes the required lifting surface geometric characteristics. Appendix D of reference (f) provides a convenient method to determine the CP location for a given planform. Note that this location must be expressed in the vehicle FS, BL, and WL coordinates and for the wing must be determined for each half of the planform. During the development and validation of this method it was found that using the CP of only the exposed portion of each planform yielded the best results.

The model for the three-dimensional C_L is based on the data presented in Section 4.1.3.3 of reference (d). The basic formulation is repeated here and the reader may refer to reference (d) for a more detailed discussion. Where possible, empirical data curves from reference (d) have been approximated with analytical functions for computational efficiency.

For the purpose of lift calculations the angle of attack range may be divided into two major subdivisions. The first or normal flow region is defined as that region where the axial velocity component is in the negative X-direction ($-90° < \alpha < 90°$); the second or reversed flow region is defined as that region where the axial component of velocity is in the positive X-direction ($-180° < \alpha < -90°$ and $90° < \alpha < 180°$). Aerodynamic calculations are similar in both regions with only the input data being different. Each of these regions may, in turn, be divided into two subregions: one for angles below $C_{L_{max}}$ ($\alpha < \alpha_b$) and one for angles above $C_{L_{max}}$ ($\alpha > \alpha_b$). Here, angle of attack, α, is defined as $\tan^{-1}$ (w/u) plus the incidence, i, of the zero lift line (average for twisted surfaces) of the surface. The following equations describe C_L for $0° \leq \alpha \leq 90°$. However, the equations hold for $-90° \leq \alpha \leq 0°$ with a sign reversal in C_L and for the reversed flow regions with the corresponding reversed flow input values and the appropriate change in angle of attack reference.

In general, C_L' is defined by:

$$C_L' = C_{L_\alpha}(\sin 2\alpha \cos \alpha/2) + C_{N_{\alpha\alpha}} \sin \alpha \cos \alpha |\sin \alpha| \tag{7}$$

where:

$$C_{L_\alpha} = K_{W(B)} \, (C_{L_\alpha})_e \, (S_e/S) \tag{8}$$

$$K_{W(B)} = 0.527(1 + d/b)^{1.534} + 0.473 \tag{9}$$

$$(C_{L_\alpha})_e = 2\pi \, AR_e/(2 + \sqrt{(2\pi AR_e/a_o)^2(1 + \tan^2 \Lambda_{1/2}) + 4}) \tag{10}$$

$$\tan \Lambda_{1/2} = \tan \Lambda_{1/4} - (4/AR) \, (0.25(1-\lambda)/(1+\lambda)) \tag{11}$$

Equation (9) represents the data of Figure 4.3.1.2-10 of reference (d). The nonlinear coefficient, $C_{N_{\alpha\alpha}}$, in equation (7) is calculated differently

Planform Geometry

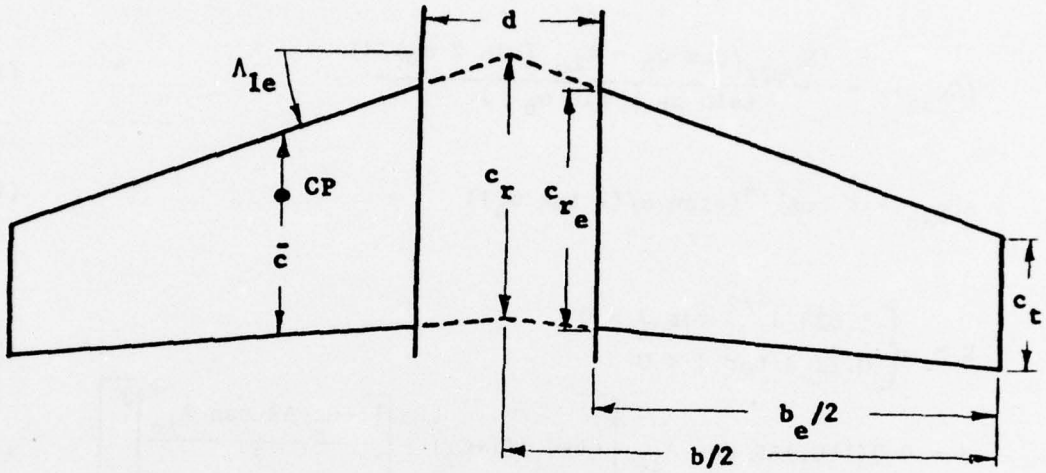

$\lambda = c_t/c_r$ $\quad AR = b^2/S$

Airfoil Incidence

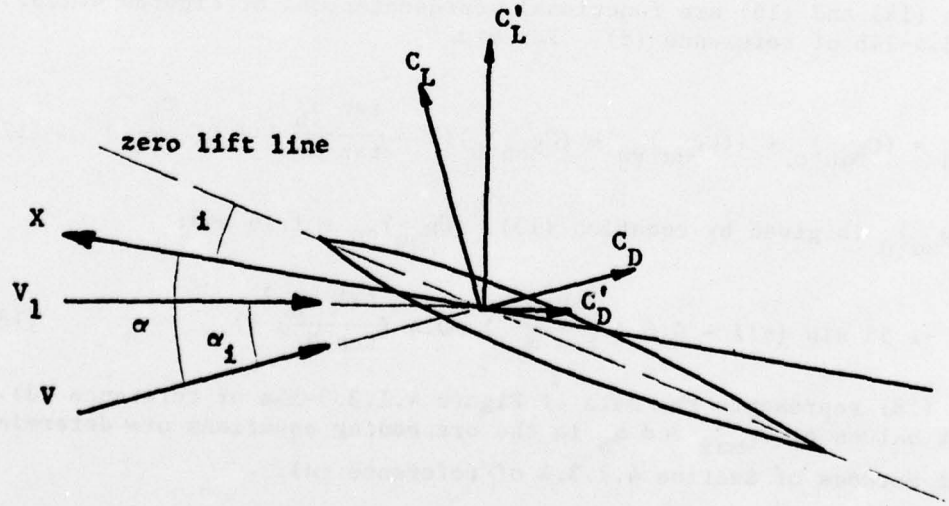

FIGURE 4: LIFTING SURFACE GEOMETRY

for the two angle of attack regions. For $\alpha \leq \alpha_b$:

$$C_{N_{\alpha\alpha}} = (C_{N_{\alpha\alpha}})_o + \Delta C_{N_{\alpha\alpha}} \tag{12}$$

where:

$$(C_{N_{\alpha\alpha}})_o = \frac{(C_{L_{max}}/\cos \alpha_b - C_{L_\alpha} (\sin 2 \alpha_b)/2)}{(\sin \alpha_b \mid \sin \alpha_b \mid)} \tag{13}$$

$$\Delta C_{N_{\alpha\alpha}} = K \cos^{2.4}(\pi \tan \alpha/(2 \tan \alpha_b)) \tag{14a}$$

$$K = \begin{cases} 1.628\ J^{1/2} & \text{for } J \geq 0 \\ 0.22\ J & \text{for } J < 0 \end{cases} \tag{14b}$$

$$J = 0.3(1+C_1)AR \cos \Lambda_{1e} \left[(1+C_1)(1+C_2) - \left[\frac{(1+C_2)AR \tan \Lambda_{1e}}{7} \right]^3 \right] \tag{15}$$

$$C_1 = 4.470\ \lambda^3 - 8.125\ \lambda^2 + 3.712\ \lambda - 0.029 \tag{16a}$$

$$C_2 = 2.943\ \lambda^3 - 7.208\ \lambda^2 + 5.199\ \lambda - 0.113 \tag{16b}$$

Equations (14) and (16) are functional representations of Figures 4.1.3.3-55a and 4.1.3.4-24b of reference (d). For $\alpha > \alpha_b$:

$$C_{N_{\alpha\alpha}} = (C_{N_{\alpha\alpha}})_o + ((C_{N_{\alpha\alpha}})_{90} - (C_{N_{\alpha\alpha}})_0)(1 - \frac{\tan \alpha_b}{\tan \alpha}) + D(\frac{C_{L_\alpha}}{2.3}) \tag{17}$$

where $(C_{N_{\alpha\alpha}})_0$ is given by equation (13), $(C_{N_{\alpha\alpha}})_{90} = 1.16$ and:

$$D = -1.55 \sin (\pi(1 - 0.6 (\frac{\tan \alpha_b}{\tan \alpha}) - 0.4 (\frac{\tan \alpha_b}{\tan \alpha})^2)) \tag{18}$$

Equation (18) represents the data of Figure 4.1.3.3-55a of reference (d). The input values of $C_{L_{max}}$ and α_b in the preceeding equations are determined using the methods of Section 4.1.3.4 of reference (d).

The lifting surface drag calculation is based on the formulation presented in reference (e) and is repeated here for completeness. For $\alpha < \alpha_b$:

$$C_D' = C_{D_o} + C_{D_\alpha}\ \alpha + C_{D_\alpha 2}\ \alpha^2 \tag{19}$$

Remember that this drag is parallel to the local velocity vector and therefore does not include induced drag. C_{D_o} is estimated using Section 4.1.5.1 of reference (d). C_{D_α} and $C_{D_{\alpha 2}}$ are normally zero for $\alpha < \alpha_b$ but may be included if available data indicates non-zero values. For $\alpha > \alpha_b$:

$$C_D' = \frac{(\alpha - \pi/2)^2 (C_{D_b} - 1.2)}{(\alpha_b - \pi/2)^2} + 1.2 \tag{20}$$

where:

$$C_{D_b} = C_{D_o} + C_{D_\alpha}\, \alpha_b + C_{D_{\alpha 2}}\, \alpha_b^2 \tag{21}$$

Equations (7), (19) and (21) represent lift and drag referenced to the direction of the local velocity which must be transformed through the induced angle of attack to yield C_L and C_D defined in the conventional manner, i.e., perpendicular and parallel to the free stream velocity vector in the x-z plane. Performing this transformation:

$$C_L = C_L' \cos \alpha_i - C_D' \sin \alpha_i \tag{22}$$

$$C_D = C_L' \sin \alpha_i + C_D' \cos \alpha_i \tag{23}$$

where:

$$\alpha_i = C_L'/(\pi AR\, e) \tag{24}$$

$$e = 0.527 + 0.1494\, AR - 0.01429\, AR^2 \tag{25}$$

Equation (25) is a functional description of the data of Figure 2.4 of reference (e) which is valid for $2 \leq AR \leq 7$. Figure 5 presents C_L and C_D for the XV-6A Kestrel wing calculated in this manner.

For a lifting surface which does not have a symmetrical airfoil section (i.e., one which produces a non-zero pitching moment at the zero lift condition) provision has been made to include C_{m_o} in the aerodynamic model. The value of C_{m_o} for a particular geometry may be estimated using the methods of Section 4.1.4.1 of reference (d). Pitch moment due to lift and drag at angle of attack is accounted for in the aero force transformation to the vehicle CG.

This completes the general description of the lift and drag model. Additional effects for each of the surfaces will now be discussed.

1. Wing

For the wing, two additional aerodynamic effects are modelled: the

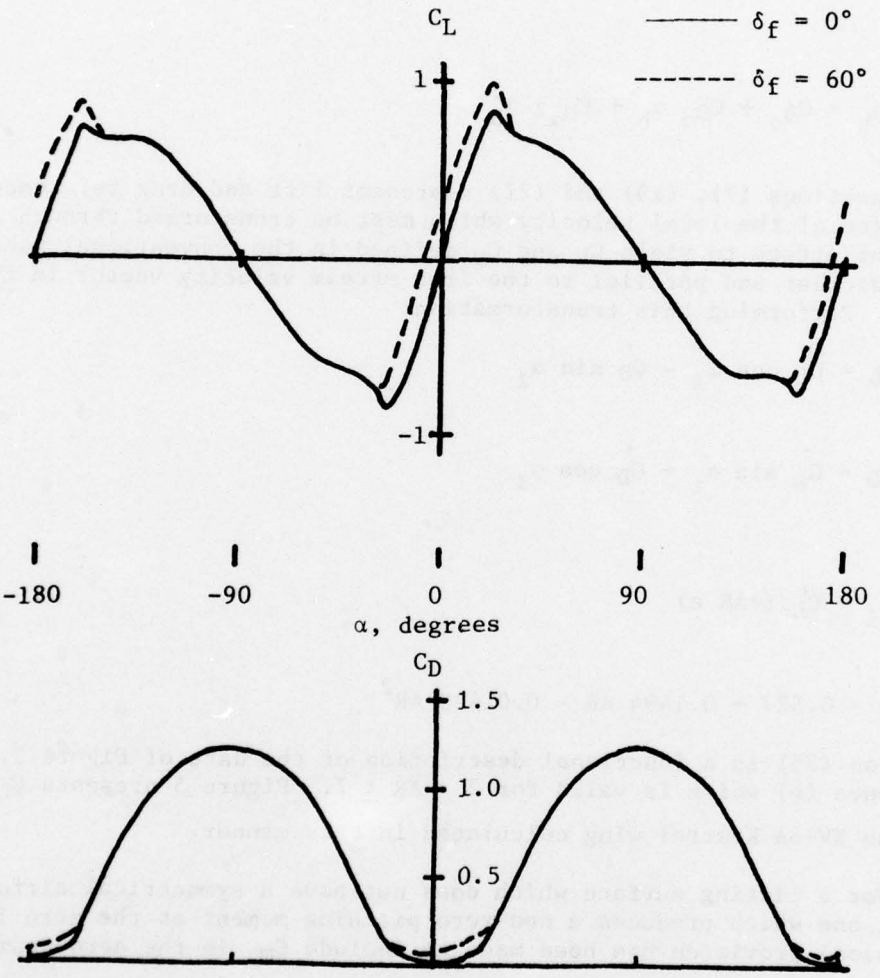

FIGURE 5: XV-6A C_L AND C_D APPROXIMATION

effect of high-lift flaps; and the effect of sideslip, roll rate and yaw rate. Deflecting a high-lift flap affects lift and drag at zero alpha, maximum lift and pitching moment. These affects are added to the basic aero model of the wing as a function of flap deflection.

$$C_{L_o} = \left(\frac{C_{L_o}}{\delta_f}\right)\delta_f \tag{26a}$$

$$\Delta C_{D_o} = \left(\frac{\Delta C_{D_o}}{\delta_f}\right)\delta_f \tag{26b}$$

$$\Delta C_{L_{max}} = \left(\frac{\Delta C_{L_{max}}}{\delta_f}\right)\delta_f \tag{26c}$$

$$\Delta C_m = C_{m_{\delta_f}}\,\delta_f \tag{26d}$$

Section 6.1 reference (d) provides methods for estimating the coefficients of equations (26). Typical flap effects, as modelled, are shown on Figure 5 for a flap deflection of 60°.

Increments in wing roll and yaw moment, L'_W and N'_W (in stability axes), due to sideslip, β; roll rate, p; and yaw rate, r; are calculated using derivatives which are estimated by the methods of reference (d), (f), or (g) and the following equations.

$$L'_W = 1/2\rho S_W b_W V_{xz}^2 \left[(C_{l_{\beta_o}} + \frac{\Delta C_{l_\beta}}{C_L} C_L)\beta + \frac{b_W}{2V_{xz}} \left(\frac{\Delta C_{l_r}}{C_L} C_L\, r + C_{l_p}\, p\right)\right] \tag{27}$$

$$N'_W = 1/2\ \rho S_W b_W\ V_{xz}^2 \left[(C_{n_{\beta_o}} + \frac{\Delta C_{n_\beta}}{C_L^2} C_L^2)\beta + \frac{b_W}{2V_{xz}} \left(\frac{\Delta C_{n_r}}{C_L^2} C_L^2 + \frac{\Delta C_{n_r}}{C_D} C_D\right)r\right.$$

$$\left. + \frac{b_W}{2V_{xz}} \left(\frac{\Delta C_{n_p}}{C_L} C_L + \frac{\Delta C_{n_p}}{C_{D_\alpha}} C_{D_\alpha}\right)p\right] \tag{28}$$

where:

$$V_{xz} = \sqrt{u^2 + w^2} \tag{29a}$$

$$\beta = \tan^{-1}\,(v/V_{xz}) \tag{29b}$$

and C_L and C_D are the averages of the left and right wing values.

Now, dimensionalizing the lift, drag, and pitch moment coefficients, and transforming the forces and moments into body axis directions yields:

$$X_{LW,RW} = 1/4\rho V_{xz}^2 S_W \left[C_L \sin(\alpha-i) - C_D \cos(\alpha-i)\right]_{LW,RW} \quad (30a)$$

$$Z_{LW,RW} = 1/4\rho V_{xz}^2 S_W \left[-C_L \cos(\alpha-i) - C_D \sin(\alpha-i)\right]_{LW,RW} \quad (30b)$$

$$M_W = 1/2\rho V_{xz}^2 S_W \bar{c}_W \left[C_{m_o} + C_{m_{\delta_f}} \delta_f\right]_W \quad (30c)$$

$$L_W = L'_W \cos(\alpha-i)_W - N'_W \sin(\alpha-i)_W \quad (30d)$$

$$N_W = L'_W \sin(\alpha-i)_W + N'_W \cos(\alpha-i)_W \quad (30e)$$

Transferring the forces and moments to the vehicle CG yields:

$$\Delta X_W = X_{LW} + X_{RW} \qquad \Delta L_W = L_W + Z_{LW}(BL_{LW} - BL_{CG}) + Z_{RW}(BL_{RW} - BL_{CG})$$

$$\Delta Y_W = 0 \qquad \Delta M_W = M_W + X_{LW}(WL_{CG} - WL_{LW}) - Z_{LW}(FS_{CG} - FS_{LW})$$

$$+ X_{RW}(WL_{CG} - WL_{RW}) - Z_{RW}(FS_{CG} - FS_{RW})$$

$$\Delta Z_W = Z_{LW} + Z_{RW} \qquad \Delta N_W = N_W - X_{LW}(BL_{LW} - BL_{CG}) - X_{RW}(BL_{RW} - BL_{CG}) \quad (31)$$

where $(FS, BL, WL)_{LW}$ and $(FS, BL, WL)_{RW}$ locate the CP's of the left and right wing panels.

2. Horizontal Stabilizer

The aerodynamics of the horizontal stabilizer are affected by the wing downwash field and the vehicle angular rates. Total effective angle of attack is assumed to be:

$$\alpha_H = \tan^{-1}(w_H/u_H) - \varepsilon + \Delta\alpha_H + i_H \quad (32)$$

where:

$$u_H = u + q(WL_{CG} - WL_H) - r(BL_H - BL_{CG}) \quad (33a)$$

$$w_H = w + p(BL_H - BL_{CG}) - q(FS_{CG} - FS_H) \quad (33b)$$

$$\varepsilon = (\varepsilon/C_{L_W})C_{L_W} \tag{34}$$

$$\Delta\alpha_H = (\varepsilon/C_{L_W})C_{L_{\alpha_W}}\dot{\alpha}_W\left(\frac{FS_H - FS_W}{u_H}\right) \tag{35}$$

Equations (33) account for induced velocities at the tail due to vehicle angular rates. Equations (34) and (35) represent corrections for wing downwash and lag of downwash, respectively. For a canard configuration, these terms would represent an upwash (i.e., $\varepsilon/C_{L_W} < 0$). The wing wake also reduces the dynamic pressure at the tail. This effect is approximated by:

$$(q_o)_H = \left(1 - \frac{\Delta q_o}{q_o}\right) 1/2\rho\ (u_H^2 + w_H^2) \tag{36}$$

where:

$$\frac{\Delta q_o}{q_o} = \left[\frac{2.42\ C_{D_o}{}^{1}/_{2}}{\frac{x'}{c} + 0.30}\right]\cos^2(\pi z'/2z_w) \tag{37}$$

$$z_w = 0.68\left[C_{D_o}\left(\frac{x'}{c} + 0.15\right)\right]^{1}/_{2} \tag{38}$$

Equation (38) for z_w is the semi-thickness of the wake. The remaining geometry is defined in Figure 6. This formulation is based on that presented in Section 4.4 of reference (d).

Body axis components of the horizontal stabilizer forces and moments at its CP, located at $(FS, BL, WL)_H$, are given by:

$$X_H = (q_o)_H\ S_H\left[C_L \sin(\alpha - i) - C_D \cos(\alpha - i)\right]_H \tag{39a}$$

$$Z_H = (q_o)_H\ S_H\left[-C_L \cos(\alpha - i) - C_D \sin(\alpha - i)\right]_H \tag{39b}$$

$$M_H = (q_o)_H\ S_H\ \bar{c}_H(C_{m_o})_H \tag{39c}$$

Referenced to the vehicle CG:

$$\Delta X_H = X_H \qquad \Delta L_H = Z_H(BL_H - BL_{CG})$$

$$\Delta Y_H = 0 \qquad \Delta M_H = M_H + X_H(WL_{CG} - WL_H) - Z_H(FS_{CG} - FS_H) \tag{40}$$

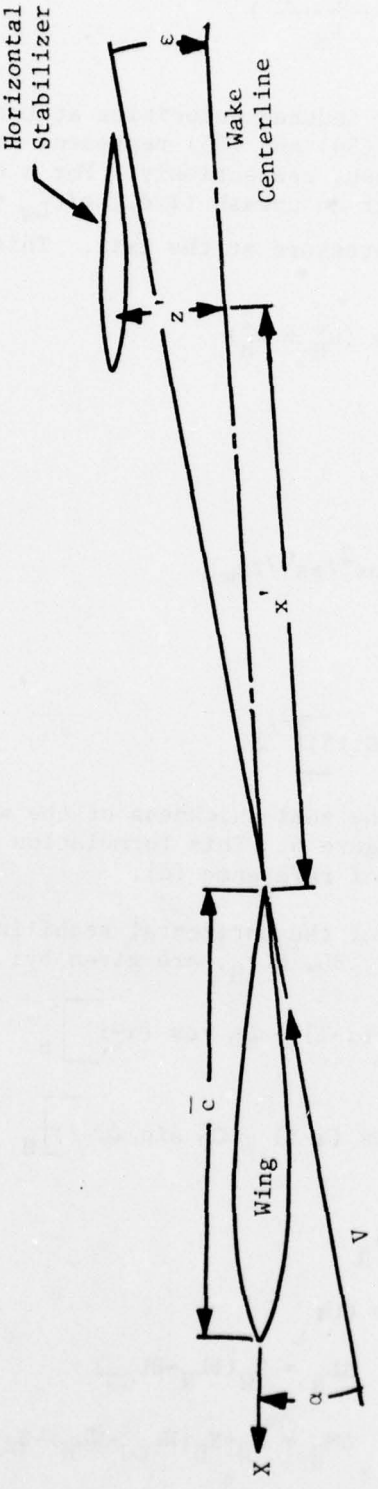

FIGURE 6: WING WAKE GEOMETRY

$$\Delta Z_H = Z_H \qquad \Delta N_H = -X_H(BL_H - BL_{CG}) \tag{40}$$

3. Vertical Stabilizer

Angle of attack of the vertical stabilizer is defined by:

$$\alpha_V = \tan^{-1}(-v_V/u_V) \tag{41}$$

where:

$$u_V = u + q(WL_{CG} - WL_V) - r(BL_V - BL_{CG}) \tag{42a}$$

$$v_V = v(1-K_v) - p(WL_{CG} - WL_V) + r(FS_{CG} - FS_V) \tag{42b}$$

The coefficient K_v in equation (42b), commonly called the sidewash coefficient, accounts for the change in lateral velocity at the vertical stabilizer due to flow around the aft fuselage. This coefficient is difficult to estimate and should be set to zero if applicable data are not available. The dynamic pressure acting on the vertical stabilizer is given by:

$$(q_o)_V = 1/2\rho(u_V^2 + v_V^2) \tag{43}$$

As for the wing and horizontal stabilizer, the vertical stabilizer forces and moments are transformed to body axis components and translated to the vehicle CG resulting in equations (44) and (45).

$$X_V = (q_o)_V S_V \left[C_L \sin(\alpha - i) - C_D \cos(\alpha - i)\right]_V \tag{44a}$$

$$Y_V = (q_o)_V S_V \left[C_L \cos(\alpha - i) + C_D \sin(\alpha - i)\right]_V \tag{44b}$$

$$N_V = (q_o)_V S_V \bar{c}_V (C_{m_o})_V \tag{44c}$$

$$\Delta X_V = X_V \qquad \Delta L_V = -Y_V(WL_{CG} - WL_V)$$

$$\Delta Y_V = Y_V \qquad \Delta M_V = X_V(WL_{CG} - WL_V)$$

$$\Delta Z_V = 0 \qquad \Delta N_V = N_V + Y_V(FS_{CG} - FS_V) - X_V(BL_V - BL_{CG}) \tag{45}$$

Control surface effects have not been discussed but are simulated by an appropriate increment in the surface angle of attack. The manner in which this increment is calculated is described in a later section of this report.

Propulsion-Induced Aerodynamics

There are at least two significant propulsion-induced aerodynamic effects which must be included in the aerodynamic model for the vehicle. The first of these is the aerodynamic interference of the propulsion system efflux in the vicinity of the airframe. This phenomenon can produce increments in the vehicle aerodynamics which are functions of engine thrust, nozzle angle and free stream velocity (magnitude and direction). Unfortunately these effects are normally very configuration dependent and the available data base is far too limited to permit complete modelling within the scope of this effort. Review of some available data on several jet-lift configurations has led, however, to the following general model approximations.

$$\frac{\Delta L_f}{T} = A_1 + (B_1 u + C_1 u^2 + D_1 u^3)\sin\theta_J \tag{46}$$

$$\frac{\Delta D}{T} = (A_2 u + B_2 u^2) \tag{47}$$

$$\frac{\Delta L}{T} = (A_3 v + B_3 v^2) \tag{48}$$

$$\frac{\Delta M}{T} = A_4 + (B_4 u + C_4 u^2 + D_4 u^3)\sin\theta_J \tag{49}$$

The coefficients in equations (46) through (49) may be derived from existing data on the subject configuration or similar configurations. Note that equations (48) and (49) represent roll and pitch moment about the vehicle CG. Transforming to body axis increments yields:

$$\Delta X_I = T\left(\frac{\Delta L_f}{T}\sin\alpha - \frac{\Delta D}{T}\cos\alpha\right) \qquad \Delta L_I = T\left(\frac{\Delta L}{T}\right)$$

$$\Delta Y_I = 0 \qquad \Delta M_I = T\left(\frac{\Delta M}{T}\right)$$

$$\Delta Z_I = T\left(-\frac{\Delta L}{T}\cos\alpha - \frac{\Delta D}{T}\sin\alpha\right) \qquad N_I = 0 \tag{50}$$

Considerable effort, both theoretical and semi-empirical, is currently being expended in this field (both in and out of ground effect) and this portion of the aerodynamic model should be updated as additional data become available.

The second interference effect is that produced by the engine (or fan) inlet momentum (ram drag). For CTOL configurations, inlet momentum primarily reduces the installed net thrust due to the ram drag effect. However, for V/STOL configurations, other significant forces and moments may also be produced due to unconventional inlet locations and large angles of attack and sideslip. Reference (h) indicates that a good approximation to inlet-

momentum-induced forces and moments is achieved by applying the inlet momentum drag, $w_a V$, in the direction of the free stream velocity at a point one inlet diameter ahead of the inlet (along the inlet axis). With this assumption, the following force and moment equations were formulated.

$$\Delta X_{RAM} = -\frac{w_a u}{g} \qquad \Delta L_{RAM} = \Delta Y_{RAM}(WL_{RAM}-WL_{CG})$$

$$\Delta Y_{RAM} = -\frac{w_a v}{g} \qquad \Delta M_{RAM} = -\Delta X_{RAM}(WL_{RAM}-WL_{CG})-\Delta Z_{RAM}(FS_{CG}-FS_{RAM})$$

$$\Delta Z_{RAM} = -\frac{w_a w}{g} \qquad \Delta N_{RAM} = \Delta Y_{RAM}(FS_{CG}-FS_{RAM}) \qquad (51)$$

The total weight flow of air through the inlet is w_a and is approximately proportional to thrust. FS_{RAM} and WL_{RAM} locate the centroid of ram drag application points for all inlets.

MASS AND INERTIAL CHARACTERISTICS

Vehicle gross weight, W, and moments of inertia, I_x, I_y, I_z, and I_{xz}, are required data for the model. The inertias are referenced to the aircraft body axis system and the weight is resolved into this system in the standard manner.

$$\Delta X_{WT} = -W \sin\theta$$

$$\Delta Y_{WT} = W \cos\theta \sin\phi$$

$$\Delta Z_{WT} = W \cos\theta \cos\phi \qquad (52)$$

θ and ϕ are the aircraft Euler angles in pitch and roll. The aircraft weight is assumed to be constant.

PROPULSION SYSTEM CHARACTERISTICS

Both fixed and vectorable nozzle engines are included in the propulsion section of the model. These nozzles are assumed to provide the primary horizontal and vertical thrust of the vehicle. If, for a given configuration, any of these nozzles are also used for active moment control, the moment control is modelled by placing reaction control jets at the same location. These jets produce only the incremental thrust for moment control and their simulation is described in a later section of this report.

Fixed Nozzle Engines

One or two fixed nozzles may be simulated. If two are simulated, they are assumed to be symmetrically located about the aircraft x-z plane, as is

normally the case. The thrust vector location is described by the FS, BL, and WL of its application point; its direction is described by yaw, ψ, and pitch, θ, relative to the x-axis (Figure 7). Body axis components of the thrust of each jet are defined by the standard axis transformation of reference (1).

$$\Delta X_{FJ} = T_{FJ} \cos\theta \cos\psi$$

$$\Delta Y_{FJ} = T_{FJ} \cos\theta \sin\psi$$

$$\Delta Z_{FJ} = -T_{FJ} \sin\theta \qquad (53)$$

Moments about the CG are given by:

$$\Delta L_{FJ} = \Delta Z_{FJ}(BL_{FJ}-BL_{CG}) - \Delta Y_{FJ}(WL_{CG}-WL_{FJ})$$

$$\Delta M_{FJ} = \Delta X_{FJ}(WL_{CG}-WL_{FJ}) - \Delta Z_{FJ}(FS_{CG}-FS_{FJ})$$

$$\Delta N_{FJ} = \Delta Y_{FJ}(FS_{CG}-FS_{FJ}) - \Delta X_{FJ}(BL_{FJ}-BL_{CG}) \qquad (54)$$

Vectorable Nozzle Engines

As many as six vectorable nozzles may be simulated within the model which has been developed. Location is again described by the FS, BL, and WL of the thrust vector application point. Two distinct means of describing the orientation of the nozzle exhaust direction are provided so that the plane of motion of the nozzle (the plane containing θ_{J_o}) may be located appropriately.

1. Roll, ϕ, about the x-axis followed by pitch, θ_{J_o}, about the displaced y-axis;
2. Yaw, ψ, about the Z-axis followed by pitch, θ_{J_o}, about the displaced Y-axis.

Figure 7 depicts the two possible orientation schemes.

Resolution of the thrust vector into body axis components differs for each orientation method. For the first method:

$$\Delta X_J = -T \sin(\theta_{J_o} + \Delta\theta_J)$$

$$\Delta Y_J = T \cos(\theta_{J_o} + \Delta\theta_J) \sin\phi$$

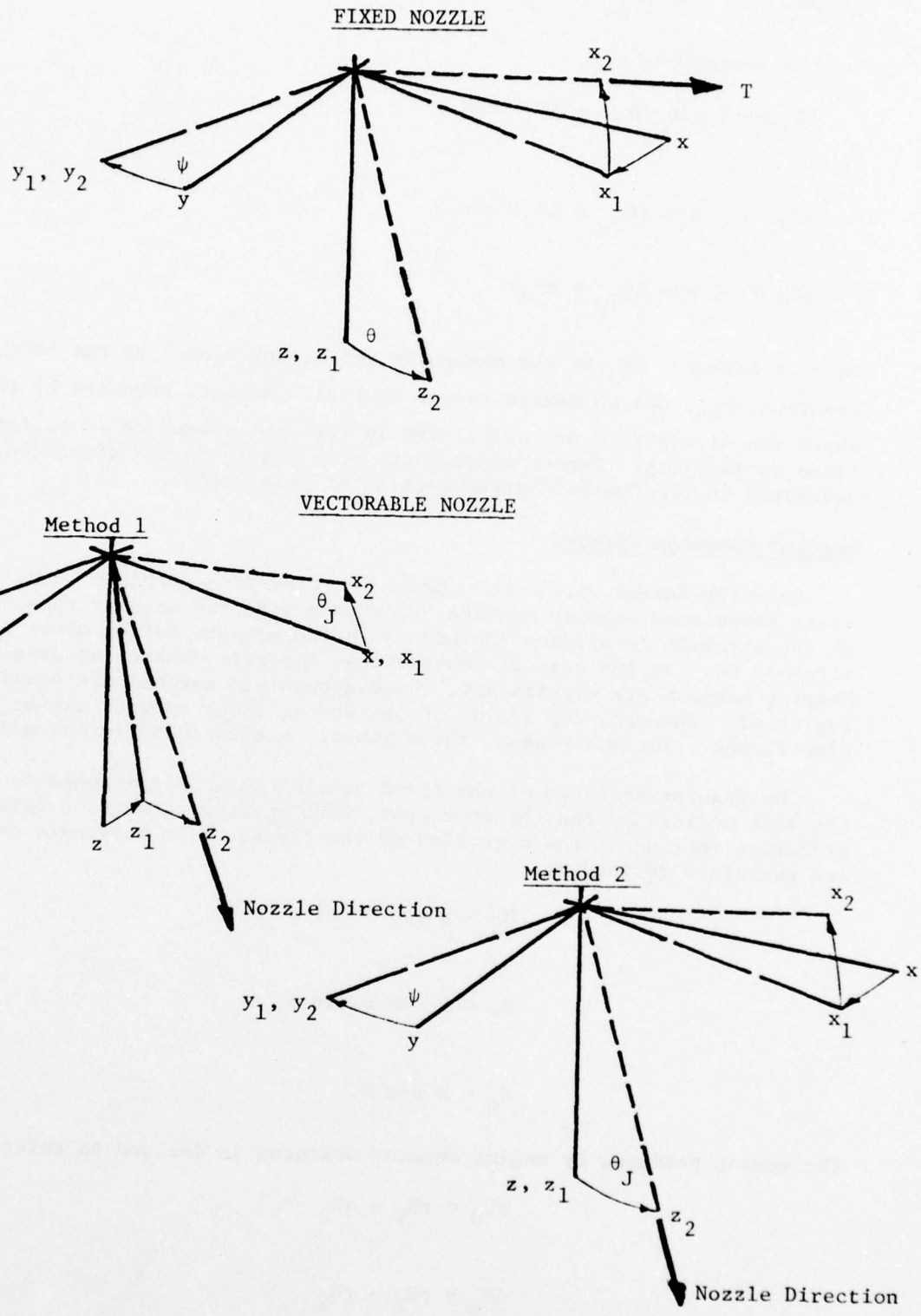

FIGURE 7: FIXED AND VECTORABLE NOZZLE ORIENTATION

$$\Delta Z_J = -T \cos (\theta_{J_o} + \Delta\theta_J) \cos \phi \qquad (55a)$$

For the second method:

$$\Delta X_J = -T \sin (\theta_{J_o} + \Delta\theta_J) \cos \psi$$

$$\Delta Y_J = -T \sin (\theta_{J_o} + \Delta\theta_J) \sin \psi$$

$$\Delta Z_J = -T \cos (\theta_{J_o} + \Delta\theta_J) \qquad (55b)$$

In both methods, $\Delta\theta_J$ is the change in jet orientation from the reference position, θ_{J_o}, due to nozzle vector control. Moments produced by these jets about the aircraft CG are calculated in the same manner as those for the fixed nozzle jets. Thrust management, both magnitude and direction, is described in the Control System section of this report.

Angular Momentum Effects

Spinning masses within the engine (compressors, turbines, etc.) and their associated angular momenta, H, couple with the angular rate of motion of the aircraft to produce increments in the moments acting about the aircraft CG. In the case of conventional aircraft, where aerodynamic damping moments are significant, these gyroscipic moments are usually neglected. However, for V/STOL at low speed, these moments may be quite significant. For this reason, these moments are included in the model.

The angular momentum of the fixed nozzle engines is assumed to be about the axis defined by the thrust vector, with positive direction being clockwise looking in the direction of the thrust. The body axis components are therefore defined by:

$$H_X = H \cos \theta \cos \psi$$

$$H_Y = H \cos \theta \sin \psi$$

$$H_Z = H \sin \theta \qquad (56)$$

The moment produced by engine angular momentum is derived in reference (f) as:

$$\Delta L_G = rH_Y - qH_Z$$

$$\Delta M_G = pH_Z - rH_X$$

$$\Delta N_G = qH_X - pH_Y \qquad (57)$$

The angular momentum of the fixed nozzle engines is assumed to be proportional to the thrust of the engine. If this assumption proves to be too gross for the engine under consideration, the model described for the vectorable nozzle engines may be used.

Since the angular momentum vector for a vectorable nozzle engine cannot be assumed to coincide with the thrust vector, a separate set of orientation angles must be defined. The angular momentum vector is located relative to the aircraft x-axis by a yaw and pitch angle in the same manner as the fixed nozzle engine thrust vector. Increments in aircraft moments are calculated in the same manner as that described for the fixed nozzle engines. The magnitude of the angular momentum is assumed to be a function of thrust defined by:

$$H = H_{max}\left(\frac{A + BT + CT^2}{100}\right) \qquad (58)$$

The coefficients A, B, and C are in units of %, %/newton and %/newton^2, respectively, and must be determined from available engine data. Angular momentum contributions are associated with each nozzle and its respective thrust when there is more than one nozzle per engine.

CONTROL SYSTEM CHARACTERISTICS

The control system model consists of longitudinal stick, lateral stick, and rudder pedals for regulation of both aerodynamic control surfaces and reaction control nozzles. In addition to these conventional controls, a thrust management system consisting of throttles and nozzle controls is also included in the model. In general, the control system model relates a total of 19 outputs to 8 inputs (Figure 8). To facilitate detailed description of the system, it is divided into three segments: Aerodynamic control, reaction control and thrust management.

Aerodynamic Control Surfaces

The effect of deflecting an aerodynamic control surface is modelled as an incremental change in angle of attack of the lifting surface of which the control surface is an integral part. For example, rudder deflection is simulated as an incremental change in vertical stabilizer angle of attack, $\Delta\alpha_V$. The longitudinal stick regulates horizontal stabilizer angle of attack, the lateral stick regulates left and right wing angle of attack and the rudder pedals regulate vertical stabilizer angle of attack. Effective angle of attack change due to control surface deflection may be estimated by applying the methods of Section 6 of reference (d). Figure 9 presents an example of the assumed form for control surface gearing and sign conventions. Note that in the case of lateral control, both $\Delta\alpha_{RW}$ and $\Delta\alpha_{LW}$ are calculated and are assumed to be equal in magnitude but opposite in direction.

Reaction Control Nozzles

Up to a maximum of ten reaction control jet nozzles are included in the model. Each nozzle is located in the aircraft axis system in a manner identical to that used for the fixed nozzle engines (FS, BL, WL, ψ and θ).

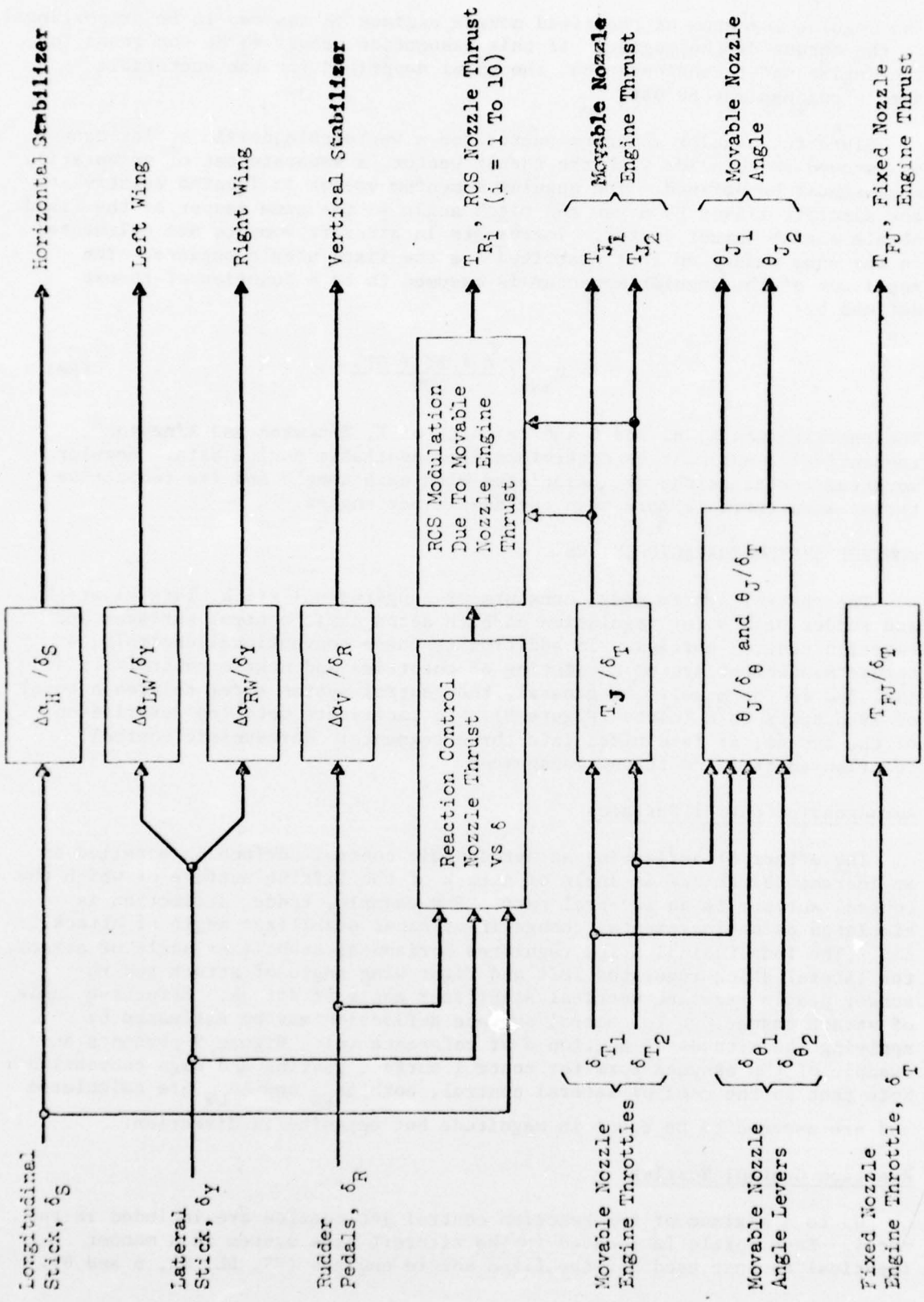

FIGURE 8: CONTROL SYSTEM MODEL SCHEMATIC

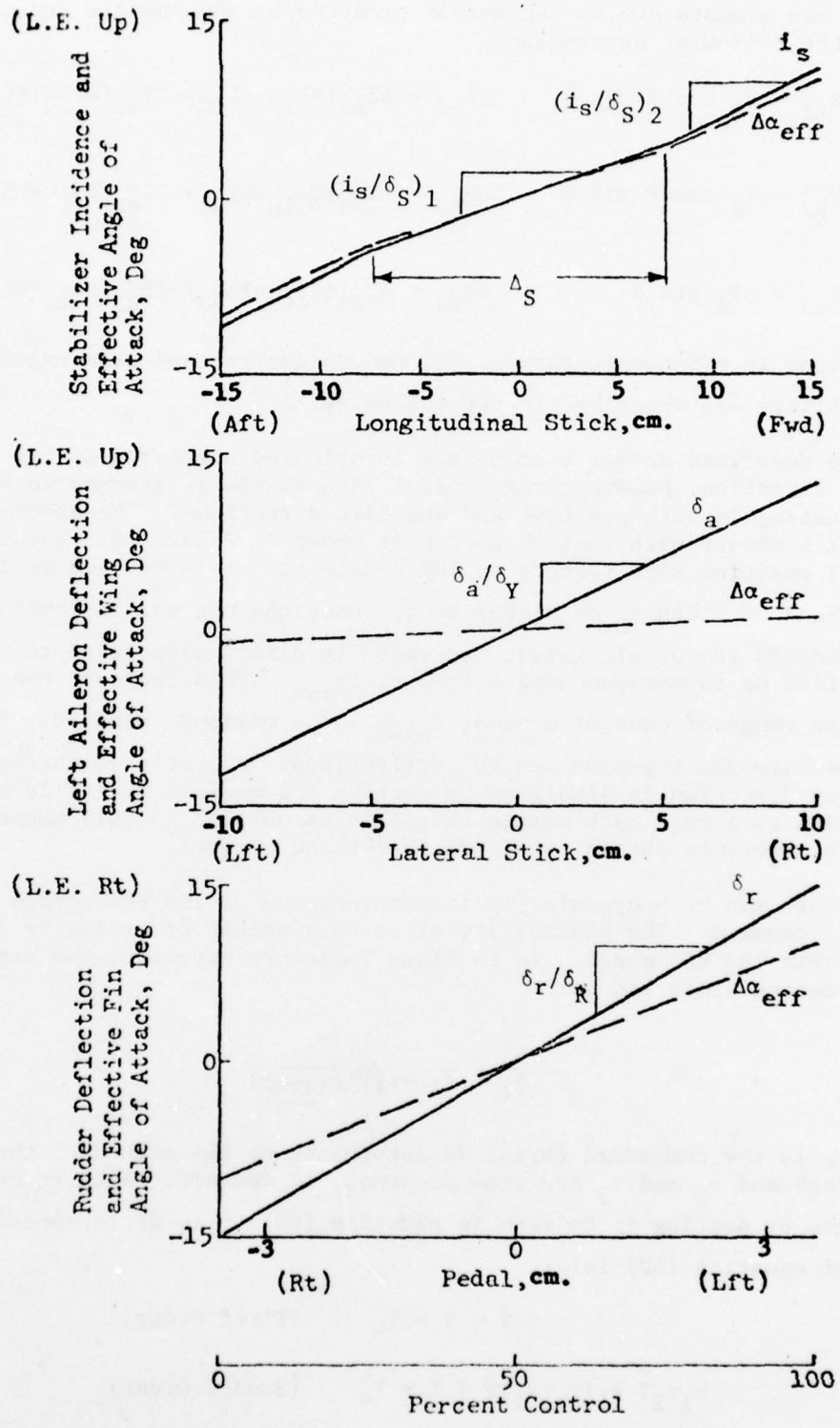

FIGURE 9: CONTROL SURFACE GEARING AND SIGN CONVENTIONS

Forces and moments due to the thrust produced by each nozzle are calculated using the following expressions.

$$\Delta X_{RJ} = T_R \cos\theta \cos\psi \qquad \Delta L_{RJ} = \Delta Z_{RJ}(BL_{RJ}-BL_{CG}) - \Delta Y_{RJ}(WL_{CG}-WL_{RJ})$$

$$\Delta Y_{RJ} = T_R \cos\theta \sin\psi \qquad \Delta M_{RJ} = \Delta X_{RJ}(WL_{CG}-WL_{RJ}) - \Delta Z_{RJ}(FS_{CG}-FS_{RJ})$$

$$\Delta Z_{RJ} = -T_R \sin\theta \qquad \Delta N_{RJ} = \Delta Y_{RJ}(FS_{CG}-FS_{RJ}) - \Delta X_{RJ}(BL_{RJ}-BL_{CG}) \qquad (59)$$

Variations in RCS nozzle thrust, T_R, due to control and main engine bleed-air availability are described in the following.

As described above, each nozzle is oriented according to its positive thrust direction; however, for control each nozzle is assumed to be capable of thrusting in both positive and negative directions. The assumed variation of nozzle thrust with control motion is shown in Figure 10. The center control position with respect to RCS nozzle thrust is defined as δ_o with a deadband of width δ_D on either side. Once the control is moved out of the deadband the nozzle thrust increases in direct proportion to control deflection up to maximum nozzle thrust, $T_{R_{max}}$. This increase takes place over the range of control motion, δ_{RAMP}. The maximum thrust may be different for positive and negative control deflections. A nozzle which thrusts in only one direction is simulated by setting the maximum thrust in the opposite direction to zero. Each nozzle thrust is calculated in this manner and then all are summed to obtain total RCS forces and moments.

There may be a dynamic lag in the response of the RCS nozzle thrust to control command. The possibility of up to a second order lag is accounted for within the RCS model. In La Place Transform notation, the expression for a second order lag is:

$$\frac{T}{T_c} = \frac{1}{(\tau_1 s+1)\ (\tau_2 s+1)} \qquad (60)$$

T_c is the commanded thrust as determined by the method of the preceeding paragraph and τ_1 and τ_2 are time constants in seconds. A first order lag is modelled by setting τ_2 to zero in equation (60). The differential equation form of equation (60) is:

$$\tau_1 \dot{T} + T = T_c \qquad \text{(First Order)} \qquad (61a)$$

$$\tau_1\tau_2 \ddot{T} + (\tau_1+\tau_2)\dot{T} + T = T_c \qquad \text{(Second Order)} \qquad (61b)$$

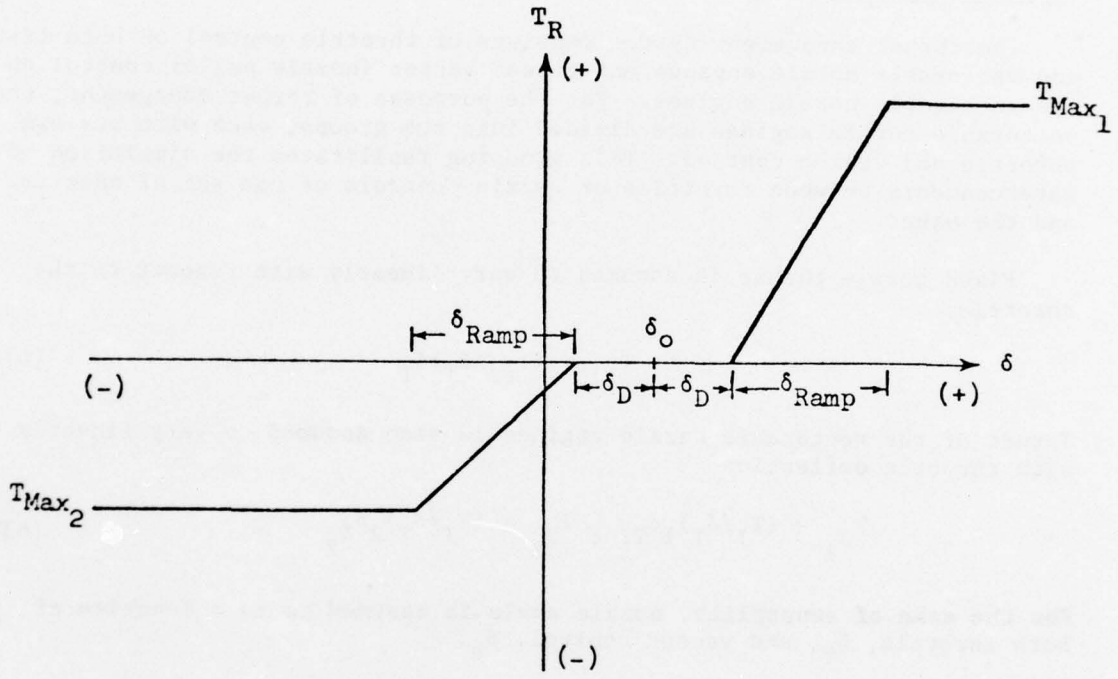

FIGURE 10: TYPICAL RCS THRUST CONTROL

Normally the RCS nozzles are powered by air which is bled from one or more of the primary engines. If this is the case, the thrust of the RCS nozzles may vary with engine thrust. This effect is approximated by:

$$(T_R)_{actual} = T_R\left(\frac{A(\Sigma T/1000) + B\,(\Sigma T/1000)^2}{100}\right) \tag{62}$$

where ΣT is the sum of the thrusts of all engines which affect the RCS and A and B are input coefficients in units of $\%/10^3$ newtons and $\%/10^6$ newtons, respectively.

Thrust Management

The thrust management system consists of throttle control on both fixed and vectorable nozzle engines and thrust vector (nozzle angle) control on the vectorable nozzle engines. For the purposes of thrust management, the vectorable nozzle engines are divided into two groups, each with its own throttle and vector control. This grouping facilitates the simulation of interconnects between throttles or nozzle controls of one set of nozzles and the other.

Fixed nozzle thrust is assumed to vary linearly with respect to the throttle.

$$T_{FJ} = (T_{FJ}/\delta_T)\delta_T \tag{63a}$$

Thrust of the vectorable nozzle engines is also assumed to vary linearly with throttle deflection.

$$T_{J_1} = (T_J/\delta_T)_1\delta_{T_1} \;;\; T_{J_2} = (T_J/\delta_T)_2\delta_{T_2} \tag{63b}$$

For the sake of generality, nozzle angle is assumed to be a function of both throttle, δ_T, and vector control, δ_θ.

$$\Delta\theta_{J_1} = (\Delta\theta_J/\delta_T)_1\delta_{T_1} + f_1(\delta_{\theta_1}) \tag{64a}$$

$$\Delta\theta_{J_2} = (\Delta\theta_J/\delta_T)_2\delta_{T_2} + f_2(\delta_{\theta_2}) \tag{64b}$$

Functions f_1 and f_2 are assumed to be piecewise linear functions of δ_{θ_1} and δ_{θ_2}, respectively.

To allow for interaction between vectorable nozzle control sets 1 and 2, the following functional relations are assumed.

$$\delta_{T_2} = A_T + B_T\delta_{T_1} + C_T\delta_{T_1}^2 \tag{65a}$$

$$\delta_{\theta_2} = A_\theta + B_\theta \delta_{\theta_1} + C_\theta \delta^2_{\theta_1} \qquad (65b)$$

Setting all coefficients to zero in either of equations (65) indicates that there is no interaction between the control sets. A typical nozzle angle interconnect schedule and the means of modelling it are shown in Figure 11.

A N A L Y S I S

Once the incremental forces and moments being generated by each of the model components are calculated as functions of the total vehicle state, they are appropriately summed and used in the following analyses. The analyses described consist of:

1. Non-linear trim calculation;
2. Stability/control derivative estimation;
3. Small perturbation stability analysis;
4. Non-linear time response calculation;
5. Least-squares vector analysis.

NON-LINEAR TRIM CALCULATION

A Newton-Raphson iteration scheme is used to determine the required control inputs and vehicle attitudes for a preselected trim state. Since the remainder of the analysis requires the vehicle to initially be in a trim condition, this calculation is essential. The iteration procedure is described first followed by definition of various possible categories of trim.

The force and moment equations for the vehicle may be expressed by:

$$F_i = f_i(x_j , V_k) \; ; \qquad \begin{matrix} i = 1, 6 \\ j = 1, 11 \\ k = 1, 6 \end{matrix} \qquad (66)$$

where the F_i are the total forces and moments calculated using the previously described model, x_j is a vector consisting of control deflections and vehicle attitudes and V_k is a vector of vehicle linear and angular velocities. The vector x_j consists of the following elements.

1. Fixed nozzle engine throttle, δ_T
2. Longitudinal stick, δ_S

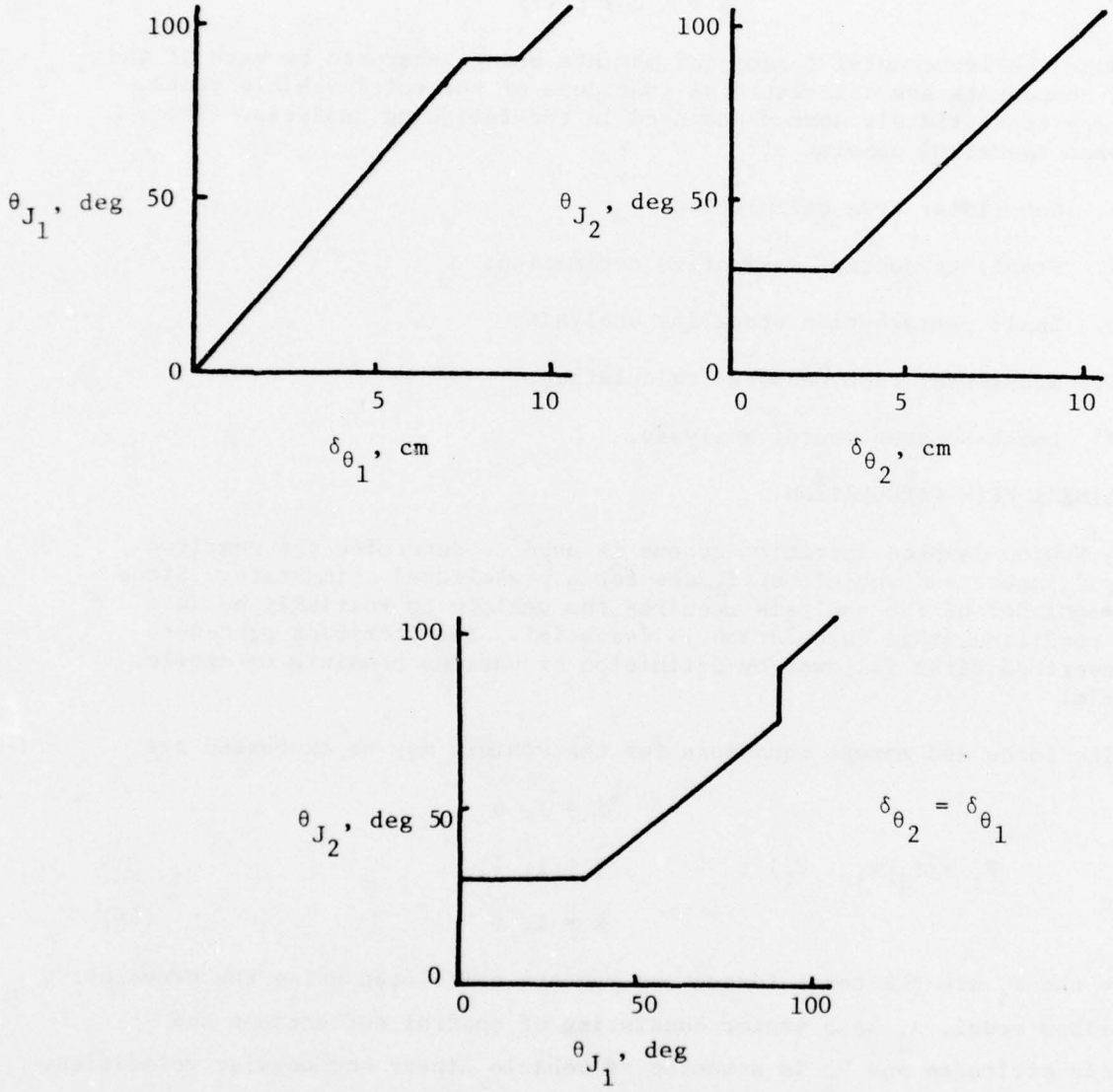

FIGURE 11: TYPICAL NOZZLE ANGLE CONTROL SCHEDULE

3. Lateral stick, δ_Y

4. Rudder pedals, δ_R

5. Yaw attitude, ψ

6. Pitch attitude, θ

7. Roll attitude, ϕ

8. Vectorable nozzle engine throttle 1, δ_{T_1}

9. Vectorable nozzle engine throttle 2, δ_{T_2}

10. Nozzle vector control 1, δ_{θ_1}

11. Nozzle vector control 2, δ_{θ_2}

The desired trim condition is specified by trim forces and moments, $(F_i)_T$, five of the eleven control variables, x_j, and the six velocity components, V_k. Care must be exercised when selecting the six control variables to be used for trim so that control is provided for each of the six degrees of freedom. With the above specification, the system to be solved for trim reduces to:

$$(F_i)_T = f_i(x_j); \qquad \begin{matrix} i = 1, 6 \\ j = 1, 6 \end{matrix} \tag{67}$$

The trim solution begins with an initial estimate of the control vector, x_{j_o}. To satisfy the specified trim condition:

$$(F_i)_T - f_i(x_{j_o} + \Delta x_j) = 0 \tag{68}$$

Therefore the trim problem reduces to solving equation (68) for Δx_j. This is accomplished by an iterative process in the following manner. $f_i(x_{j_o} + \Delta x_j)$ is expanded with second and higher order terms neglected yielding:

$$(F_i)_T - f_i(x_{j_o}) - \left(\frac{\partial f_i}{\partial x_j} \bigg|_{x_{j_o}} \right) \Delta x_j = 0 \tag{69}$$

Solving for Δx_j:

$$\Delta x_j = \left(\frac{\partial f_i}{\partial x_j}\bigg|_{x_{jo}}\right)^{-1} \underbrace{((F_i)_T - f_i(x_{jo}))}_{\Delta F_i} \tag{70}$$

$\left(\frac{\partial f_i}{\partial x_j}\bigg|_{x_{jo}}\right)$ is a six-by-six matrix evaluated at x_{jo} and is calculated using a difference technique

$$\left(\frac{\partial f_i}{\partial x_j}\bigg|_{x_{jo}}\right) = \frac{f_i(x_{jo} + \delta x_j) - f_i(x_{jo})}{\delta x_j} \tag{71}$$

The magnitude of δx_j is assumed to be 1/2 of the maximum allowable change in Δx_j per iteration. Note that if the matrix of equation (71) is singular (inverse does not exist) a trim solution cannot be obtained using the six selected control variables.

After Δx_j is calculated, a new control vector estimate, $x_{j_1} = x_{jo} + \Delta x_j$, is made. The increment Δx_j is limited by a preselected maximum value which decreases as ΔF_i approaches zero (as a trim solution is approached). This improves the convergence of the iteration scheme when severe nonlinearities are present. The process is repeated until ΔF_i is within allowable limits. At this point, the current value of x_j is the trim solution for the control vector.

The allowable trim conditions which have been considered may be grouped into three categories:

1. Trim with zero angular rate;
2. Push-overs and pull-ups;
3. Coordinated turns.

The required trim forces and moments, $(F_i)_T$, are calculated by substituting the appropriate velocities and accelerations into equations (72).

$$X_T = m\dot{u} + qw - rv \tag{72a}$$

$$Y_T = m\dot{v} + ru - pw \tag{72b}$$

$$Z_T = m\dot{w} + pv - qu \tag{72c}$$

$$L_T = qr(I_z - I_y) - pq\, I_{xz} \tag{72d}$$

$$M_T = pr(I_x - I_z) + (p^2 - r^2)I_{xz} \tag{72e}$$

$$N_T = pq(I_y - I_x) + qr\, I_{xz} \tag{72f}$$

STABILITY/CONTROL DERIVATIVE ESTIMATION

After trim has been established, the aircraft stability derivatives may be evaluated at the trim point. These derivatives indicate the sensitivity of the aircraft body axis forces and moments to incremental changes in the body axis linear and angular velocities. Each velocity is incremented and the resulting changes in the forces and moments are calculated. The stability derivatives are formed by dividing the force and moment increments by the corresponding velocity increments.

The accuracy of this calculation is directly dependent upon the value chosen for the velocity increments. Too small a value might result in errors due to small differences in large numbers; too large a value might overlook the effect of localized non-linearities. A good rule of thumb to use in determining the increment is to use 2 percent of the trim velocity for linear velocity increments and 0.3 percent of the trim velocity (in metres/second) for angular velocity increments (in units of radians per second). These increments result in approximately 1 degree increments in the individual surface angles of attack.

The control derivatives are calculated using equation (71) in the same manner used during the trim iterations.

SMALL PERTURBATION STABILITY ANALYSIS

The derivatives described in the preceeding paragraphs may be used in a linearized, small perturbation aircraft stability analysis. The present method uses the standard 3 DOF uncoupled analysis as developed in Flight Dynamics references such as reference (f). The equations which form the basis of the analysis are presented in Table III. These equations are formulated in a stability axis reference frame with the controls fixed. Trim sideslip and flight path angle are assumed to be zero and, therefore, these equations are valid only when these assumptions are satisfied by the trim condition. The acceleration derivatives ($Z'_{\dot{w}}$ and $M'_{\dot{w}}$) appearing in Table III are defined by:

$$Z'_{\dot{w}} = 1/2\rho S_H(FS_H - FS_{CG})(C_{L_\alpha})_H(C_{L_\alpha})_W(\varepsilon/C_{L_W}) \tag{73a}$$

$$M'_{\dot{w}} = (FS_H - FS_{CG})Z'_{\dot{w}} \tag{73b}$$

TABLE III

THREE DEGREE OF FREEDOM SMALL PERTURBATION EQUATIONS

LONGITUDINAL

X Equation : $(ms - X'_{\dot{u}})\, u/V + (-X'_{w})\, \alpha + 1/V(-X'_{q}s + mg)\, \theta = 0$

Z Equation : $(-Z'_{\dot{u}})\, u/V + ((m - Z'_{\dot{w}})s - Z'_{w})\, \alpha + 1/V((-mV - Z'_{q})s)\, \theta = 0$

M Equation : $(-M'_{\dot{u}})\, u/V + (-M'_{\dot{w}}s - M'_{w})\, \alpha + 1/V(I'_{y}s^{2} - M'_{q}s)\, \theta = 0$

LATERAL

Y Equation : $(ms - Y'_{\dot{v}})\, \beta + 1/V(-Y'_{p}s - mg)\, \phi + 1/V(mV - Y'_{r})\, r = 0$

L Equation : $(-L'_{\dot{v}})\, \beta + 1/V(I'_{x}s^{2} - L'_{p}s)\, \phi + 1/V(-I'_{xz}s - L'_{r})\, r = 0$

N Equation : $(-N'_{\dot{v}})\, \beta + 1/V(-I'_{xz}s^{2} - N'_{p}s)\, \phi + 1/V(I'_{z}s - N'_{r})\, r = 0$

The calculated stability derivatives must be transformed to stability axes for use in the equations of Table III. This is easily accomplished using the method of Appendix B of reference (f) or another similar reference.

The characteristics equations for both longitudinal and lateral degrees of freedom are formulated from the equations of Table III and solved for the characteristic roots. Common control transfer functions may also be calculated. This procedure has been automated and is described in Volume II of this report.

NON-LINEAR TIME RESPONSE CALCULATION

Once trim has been established, the aircraft model may be "flown" through a time dependent trajectory which is driven by a combination of input forcing functions (e.g., control motion, gust disturbance, etc.). The maneuver time history is computed by integrating the fully coupled, six DOF equations of motion of the vehicle (Table IV); recomputing the vehicle non-linear forces and moments at each time step. A four-cycle Runge-Kutta technique is used to perform the necessary integrations.

LEAST-SQUARES VECTOR ANALYSIS

A simplified, least-squares trigonometric curve fit is included in the programmed analyses to facilitate amplitude and phase angle analyses of oscillatory vehicle behavior. Portions of the time history output of the program are fit using general equations of the form:

$$x = C_1 \sin \omega t + C_2 \cos \omega t + C_3 \tag{74}$$

Coefficients C_1, C_2, and C_3 are determined by solving the following three simultaneous equations when N data points of the form (x_i, t_i) are available and frequency, ω, is assumed.

$$\Sigma x_i = C_1 \Sigma \sin \omega t_i + C_2 \Sigma \cos \omega t_i + NC_3 \tag{75a}$$

$$\Sigma x_i \sin \omega t_i = C_1 \Sigma \sin^2 \omega t_i + C_2 \Sigma \sin \omega t_i \cos \omega t_i + C_3 \Sigma \sin \omega t_i \tag{75b}$$

$$\Sigma x_i \cos \omega t_i = C_1 \Sigma \sin \omega t_i \cos \omega t_i + C_2 \Sigma \cos^2 \omega t_i + C_3 \Sigma \cos \omega t_i \tag{75c}$$

Amplitude and phase are determined by:

$$\text{Amplitude} = (C_1^2 + C_2^2)^{1/2} \tag{76a}$$

$$\text{Phase} = \tan^{-1}(C_2/C_1) \tag{76b}$$

TABLE IV

SIX DEGREE OF FREEDOM EQUATIONS OF MOTION

$$\dot{u} = \frac{X}{m} + rv - qw - g \sin\theta$$

$$\dot{v} = \frac{Y}{m} + pw - ru + g \cos\theta \sin\phi$$

$$\dot{w} = \frac{Z}{m} + qu - pv + g \cos\theta \cos\phi$$

$$\dot{p} = \frac{I_z}{I_x I_z - I_{xz}^2} \left[L + \frac{I_{xz}}{I_z} (N - qr\, I_{xz}) - qr\,(I_z - I_y) + pq\, I_{xz} \left(1 - \frac{I_y - I_x}{I_z}\right) \right]$$

$$\dot{q} = \frac{1}{I_y} \left[M - I_{xz}\,(p^2 - r^2) - rp\,(I_x - I_z) \right]$$

$$\dot{r} = \frac{I_x}{I_x I_z - I_{xz}^2} \left[N + \frac{I_{xz}}{I_x} (L + pq\, I_{xz}) - pq\,(I_y - I_x) - qr\, I_{xz} \left(1 - \frac{I_z - I_y}{I_x}\right) \right]$$

$$\dot{\psi} = (q \sin\phi + r \cos\phi) \sec\theta$$

$$\dot{\theta} = q \cos\theta - r \sin\phi$$

$$\dot{\phi} = p + q \sin\phi \tan\theta + r \cos\phi \tan\theta$$

$$\begin{bmatrix} \dot{x} \\ \dot{y} \\ \dot{z} \end{bmatrix} = \begin{bmatrix} \cos\theta \cos\psi & \cos\theta \sin\psi & -\sin\theta \\ \sin\phi \sin\theta \cos\psi - \cos\phi \sin\psi & \sin\phi \sin\theta \sin\psi + \cos\phi \cos\psi & \sin\phi \cos\theta \\ \cos\phi \sin\theta \cos\psi + \sin\phi \sin\psi & \cos\phi \sin\theta \sin\psi - \sin\phi \cos\psi & \cos\phi \cos\theta \end{bmatrix} \begin{bmatrix} u \\ v \\ w \end{bmatrix}$$

V A L I D A T I O N

In order to validate the models and methods described in this report, the XV-6A Kestrel (Figure 12) was modelled using basic geometry and aerodynamic data and analyzed using the computerized prediction method. The results were compared with existing wind tunnel and flight test data from references (j), (k), and (l). In general, the results correlated reasonably well with the reference data.

Appendix A contains a description of the model input data used and some of the data comparisons resulting from the validation analysis.

C O N C L U S I O N S A N D R E C O M M E N D A T I O N S

A six DOF V/STOL Stability and Control modelling and prediction method has been developed, computerized and validated with existing vehicle wind tunnel and flight test data. The method is capable of analyzing both static and dynamic characteristics of jet lift and lift/cruise fan V/STOL configurations in hover and transition flight. The method is most suited to a preliminary design environment where wind tunnel data are not available or are incomplete.

As additional data become available on V/STOL configurations, further validation should be attempted and modifications should be made to the method, if warranted, to enhance its versatility and credibility.

WING:	Span	6.98 m
	Area	17.32 m^2
	MAC	2.64 m
	AR	2.81
LENGTH:		12.01 m
MAX HEIGHT:		3.30 m

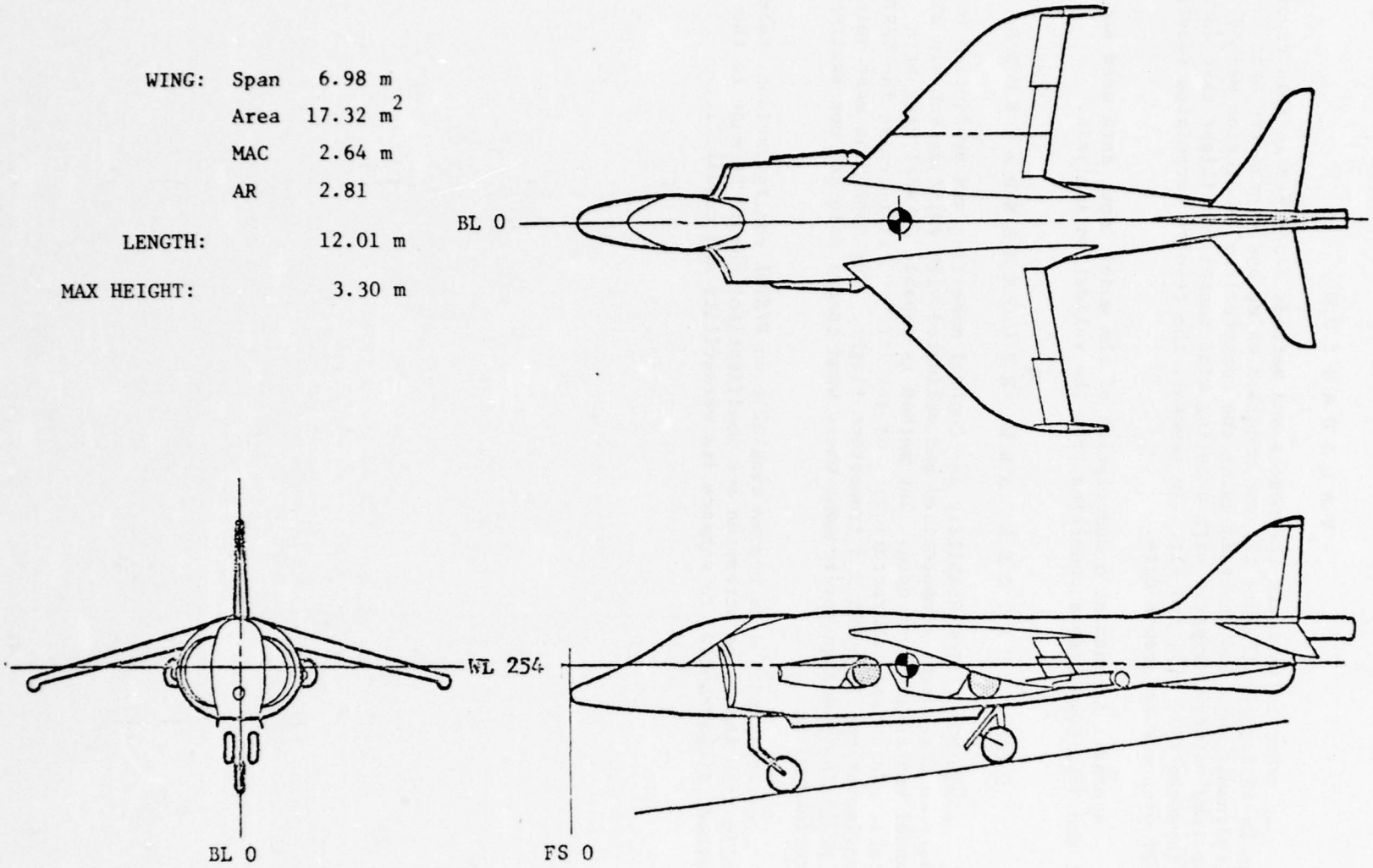

FIGURE 12: XV-6A KESTREL, 3-VIEW

NADC-76312-30

REFERENCES

(a) Livingston, Charles L., "A Stability and Control Prediction Method for Helicopters and Stoppable Rotor Aircraft", Air Force Flight Dynamics Laboratory, Air Force Systems Command, Wright-Patterson Air Force Base, Ohio, AFFDL-TR-69-123, Volumes 1 through 4, February 1970.

(b) Mazza, C. J., Brennan, T. J., Siewert, R. F., et. al., "U. S. Navy V/STOL Technology Assessment", Naval Air Systems Command, June 1975.

(c) Martin, G. L., "A Method and Program for the Calculation of Store Free-Stream Aerodynamic Coefficients", GAC Aerodynamics Section Technical Data Report No. 391-70-5, August 1971.

(d) Hoak, D. E., et. al., "USAF Stability and Control DATCOM", Flight Control Division, AFFDL, Wright-Patterson AFB, Ohio, October 1960 (Revised January 1975).

(e) Roskam, J., Methods for Estimating Drag Polars of Subsonic Airplanes, published by the author, Lawerence, Kansas, 1973.

(f) Etkin, B., Dynamics of Flight, John Wiley and Sons, Inc., New York, 1959.

(g) Perkins, C. D., and Hage, R. E., Airplane Performance, Stability and Control, John Wiley and Sons, Inc., New York, 1949.

(h) Kuhn, R. E. and McKinney, M. O., "NASA Research on the Aerodynamics of Jet VTOL Engine Installations, AGARD paper, October 1965.

(i) Thelander, J. A., "Aircraft Motion Analysis", AFFDL, FDL-TDR-64-70, Wright-Patterson Air Force Base, Ohio, March 1965.

(j) McKinzie, G. A., et. al., "P1127 (XV-6A) V/STOL Handling Qualities Evaluation", AFFTC, TR68-10, Edwards Air Force Base, California, August 1968.

(k) Margason, R. J., et. al., "Wind Tunnel Investigation at Low Speed of a Model of the Kestrel (XV-6A) Vectored-Thrust V/STOL Airplane", Langley Research Center, NASA TN D-6826, July 1972.

(l) McGregor, D. M., "A Flight Investigation of Various Stability Augmentation System for a Jet-Lift V/STOL Aircraft (P1127) Using an Airborne Simulator", NAE/NRC Aero Report LR-500, February 1968.

LIST OF SYMBOLS

Symbol	Description	Units
a_o	2-D Lift Curve Slope	1/rad
A	Axial Force	N (lb)
A, B, C, D	Miscellaneous coefficients	-
AR	Aspect Ratio, b^2/S	-
b	Span	m (ft)
BL	Butt Line, positive on right side of aircraft	cm (in)
$\bar{c}$	Mean Aerodynamic Chord	m (ft)
c_r	Root Chord	m (ft)
c_t	Tip Chord	m (ft)
C_D	Drag coefficient, D/q_oS, parallel to free stream velocity	-
C_D'	Drag coefficient, D'/q_oS, parallel to local velocity	-
C_{D_o}	Drag Coefficient at Zero Lift	-
C_{D_α}	Change in profile drag with angle of attack	1/rad
$C_{D_\alpha}{}^2$	Change in profile drag with angle of attack squared	$1/rad^2$
CG	Center of Gravity	-
C_{l_p}	Roll moment coefficient due to roll rate	1/rad
C_{l_r}	Roll moment coefficient due to yaw rate	1/rad
C_{l_β}	Roll moment coefficient due to sideslip	1/rad
C_L	Lift coefficient perpendicular to free stream velocity, L_f/q_oS	-
C_L'	Lift coefficient perpendicular to local velocity, L_f'/q_oS	-

LIST OF SYMBOLS (Continued)

Symbol	Description	Units
C_{L_α}	Change in lift coefficient with angle of attack	1/rad
C_{m_o}	Zero lift pitch moment coefficient, $M/q_o S\bar{c}$	-
$C_{m_{\delta_f}}$	Pitch moment due to flap deflection	1/deg
C_{n_p}	Yaw moment coefficient due to roll rate	1/rad
C_{n_r}	Yaw moment coefficient due to yaw rate	1/rad
C_{n_β}	Yaw moment coefficient due to sideslip	1/rad
$C_{N_{\alpha\alpha}}$	Non-linear normal force coefficient	$1/rad^2$
CP	Center of aerodynamic pressure	-
d/b	Ratio of body diameter to span	-
D	Drag force parallel to free stream velocity, positive in direction of velocity	N (lb)
e	Oswald efficiency factor	-
FS	Fuselage Station, positive aft	cm (in)
F_i	General force or moment	N (lb) or N.m (ft.lb)
g	Acceleration of gravity	m/sec^2 (ft/sec^2)
H	Angular momentum	$kg.m^2/sec$ ($slug.ft^2/sec$)
i	Lifting surface incidence to fuselage x-axis	deg
I_x, I_y, I_z	Moments of inertia about body x, y, and z axes	$kg.m^2$ ($slug.ft^2$)
I_{xz}	Product of inertia	$kg.m^2$ ($slug.ft^2$)
K_v	Sidewash coefficient	-
$K_{W(B)}$	Wing/body interference factor	-

LIST OF SYMBOLS (Continued)

Symbol	Description	Units
L, M, N	Body axis roll, pitch and yaw moments	N.m (ft.lb)
L_f	Lift force perpendicular to free stream velocity vector	N (lb)
m	Mass	kg (slug)
MAC	Mean Aerodynamic Chord	m (ft)
n_i	Exponents in fuselage aero approximations	-
N_f	Normal force, positive in negative z-direction	N (lb)
p, q, r	Body axis roll, pitch and yaw rates	rad/sec
q_o	Dynamic pressure, $1/2\rho V^2$	N/m^2 (lb/ft^2)
s	La Place operator	1/sec
S	Planform area	m^2 (ft^2)
t	Time	sec
T	Thrust	N (lb)
T_c	Commanded thrust	N (lb)
$[T]$	Euler transformation matrix	-
u, v, w	Body axis x, y, and z velocities	m/sec (ft/sec)
V	Total velocity	m/sec (ft/sec)
w_a	Inlet air weight flow	N/sec (lb/sec)
W	Weight	N (lb)
WL	Water Line, positive up	cm (in)
x_j	Control vector	-
x'	Distance from wing trailing edge to horizontal stabilizer quarter-chord, measured along wing wake centerline	m (ft)

LIST OF SYMBOLS (Continued)

Symbol	Description	Units
X, Y, Z	Forces in the x, y, and z body axis directions	N (lb)
z_w	Wing wake semi-width at horizontal stabilizer location	m (ft)
z'	Normal distance from wing wake centerline to horizontal stabilizer	m (ft)
α	Angle of attack, $\tan^{-1}(w/u)$	deg
α_b	Angle of attack corresponding to $C_{L_{max}}$	deg
α_i	Induced angle of attack	deg
α_T	Total angle of attack, $\tan^{-1}(v^2+w^2)^{1/2}/u)$	deg
α_y	Yaw angle of attack, $\tan^{-1}(v/u)$	deg
α_1, α_2	Angles of attack corresponding to maximum fuselage moments	deg
β	Sideslip angle, $\sin^{-1}(v/V)$	deg
δ_a	Aileron deflection, positive for left wing trailing edge down	deg
δ_D	Semi-width of RCS controller dead band	deg
δ_e	Elevator deflection, positive for trailing edge down	deg
δ_f	Wing flap deflection	deg
δ_r	Rudder deflection, positive for trailing edge left	deg
δ_R	Rudder pedal deflection, positive for left pedal	cm (in)
δ_{RAMP}	RCS versus δ ramp length	cm (in)
δ_S	Longitudinal stick deflection, positive for forward stick	cm (in)

LIST OF SYMBOLS (Continued)

Symbol	Description	Units
δ_T	Fixed nozzle engine throttle deflection	cm (in)
δ_{T_1}, δ_{T_2}	Vectorable nozzle engine throttle deflection	cm (in)
δ_Y	Lateral stick deflection, positive for right stick	cm (in)
δ_o	RCS controller center position	cm (in)
δ_{θ_1}, δ_{θ_2}	Vectorable nozzle angle controller deflection	cm (in)
ε	Downwash angle	deg
θ_J	Nozzle angle	deg
λ	Taper ratio, c_t/c_r	-
Λ_n	Sweep angle of the n^{th} fractional chord line	deg
ρ	Atmospheric density	kg/m^3 ($slug/ft^3$)
τ_i	Time constant	sec
ψ, θ, ϕ	Euler yaw, pitch, and roll angles	deg
ω	Frequency	rad/sec

Subscripts

CG	Referenced to vehicle center of gravity
e	Property of exposed portion of planform
F	Fuselage parameter
FJ	Fixed nozzle engine parameter
G	Gyroscopic (angular momentum) effect
H	Horizontal stabilizer parameter
I	Propulsion induced aero effect
J	Vectorable nozzle engine parameter

LIST OF SYMBOLS (Continued)

Subscripts	Description
le	Referenced to planform leading edge
LW	Left wing parameter
max	Local maximum value
o	Reference condition
RAM	Inlet momentum effect
R, RJ	Reaction jet parameter
RW	Right wing parameter
T	Trim condition
V	Vertical stabilizer parameter
WT	Weight component
W	Total wing parameter
X	X body axis component
xy	Component in x-y plane
xz	Component in x-z plane
Y	Y body axis component
Z	Z body axis component

Mathematical Symbols

$\Delta(\ )$	Incremental quantity
$(\ )'$	Stability axis quantity
$(\dot{\ }), (\ddot{\ })$	First and second time derivatives
X_y	Partial derivative of X with respect to y
$(\ )^{-1}$	Matrix inverse
$(\ )^T$	Matrix transpose
$(\ )\big\|_x$	Quantity evaluated at x

A P P E N D I X A

VALIDATION MODEL AND RESULTS

To validate both the modelling technique and the calculative procedures which are described in this report, an existing V/STOL configuration was modelled and the resulting predictions were compared with flight test results. Because of data availability, the XV-6A Kestrel (Figure A-1) was selected to be the sample configuration. The scope of the validation was limited by the available flight data. Physical characteristics of the XV-6A were taken from reference (j) and basic aerodynamic data were taken from reference (k).

The vehicle model input is presented in five sections: (1) weight and inertia characteristics; (2) fuselage aerodynamics; (3) wing and empennage aerodynamics; (4) propulsion system characteristics and propulsion induced aerodynamics; (5) control system characteristics. Data for each model subsection are described in detail in the following.

The nominal vehicle weight, CG, and inertias are listed in Table A-I.

TABLE A-I
XV-6A WEIGHT AND INERTIAS

Gross Weight: 53,379 N

Inertias: I_x = 5016 kg.m^2

I_y = 30,370 kg.m^2

I_z = 32,946 kg.m^2

I_{xz} = 2300 kg.m^2

CG location (10.2%$\bar{c}$): FS 556.8
BL 0
WL 251.0

Fuselage aerodynamics were estimated using the method of reference (c) for the complete angle of attack and sideslip range. The estimated aerodynamics were approximated with the functions described in this report. Figure A-2 graphically presents both the estimated and curve fit data and Table A-II lists the functional expressions which were used for the validation calculations.

Wing and empennage geometrical data and basic aerodynamic characteristics are listed in Table A-III. The downwash and flap effects were calculated using Sections 4.4 and 6.1 of reference (d). The lateral/directional effects were estimated using the charts and methods of Appendix B of reference (f).

The XV-6A aircraft is powered by the Rolls Royce/Bristol Pegasus 5 fan lift/thrust engine. Exhaust gas (both fan and turbine) is forced through four swivelling nozzles--two on each side of the fuselage producing approximately

Wing:	Span	6.98 m
	Area	17.32 m^2
	MAC	2.64 m
	AR	2.81
Length:		12.01 m
Height:		3.30 m

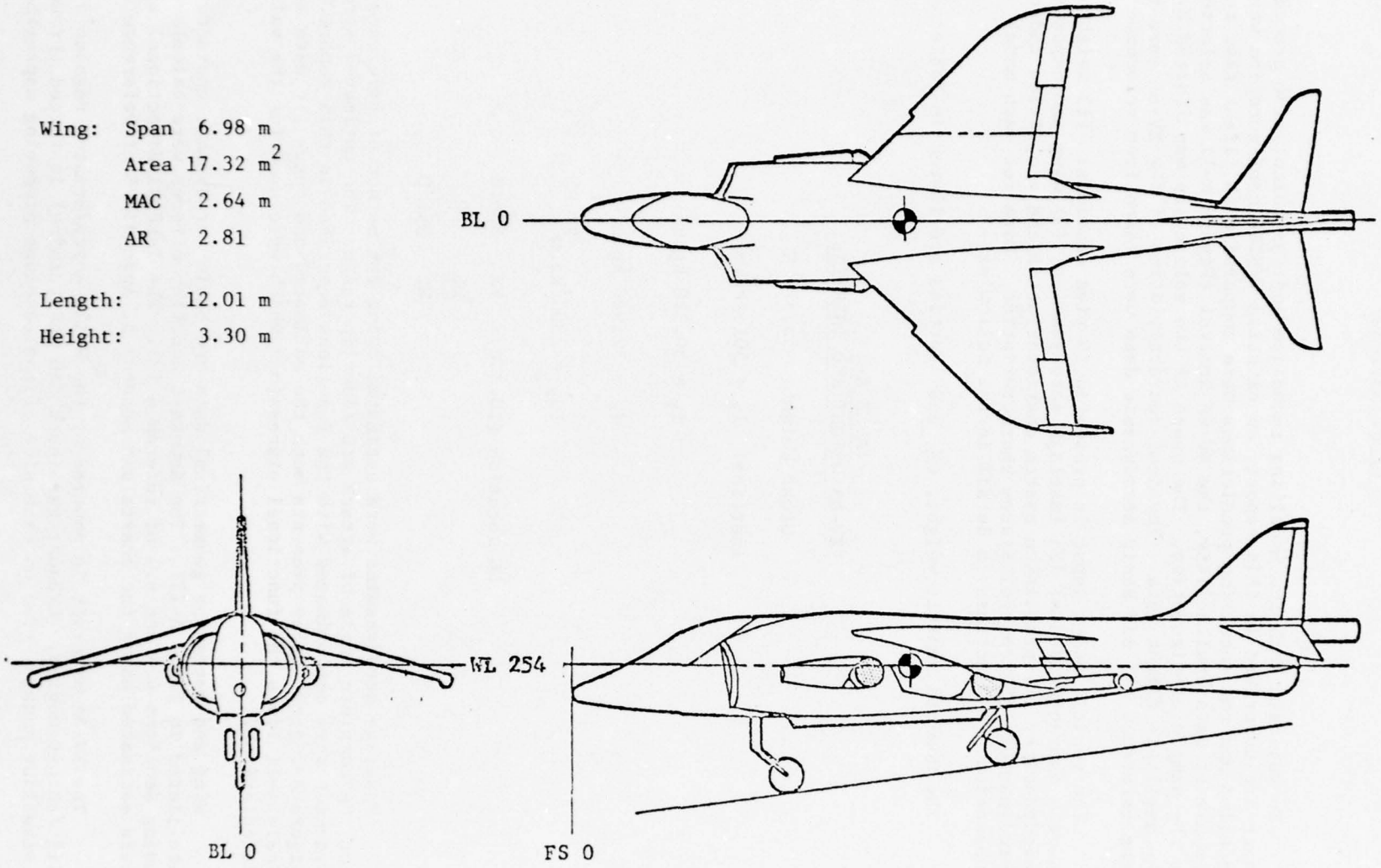

FIGURE A-1: XV-6A KESTREL, 3-VIEW

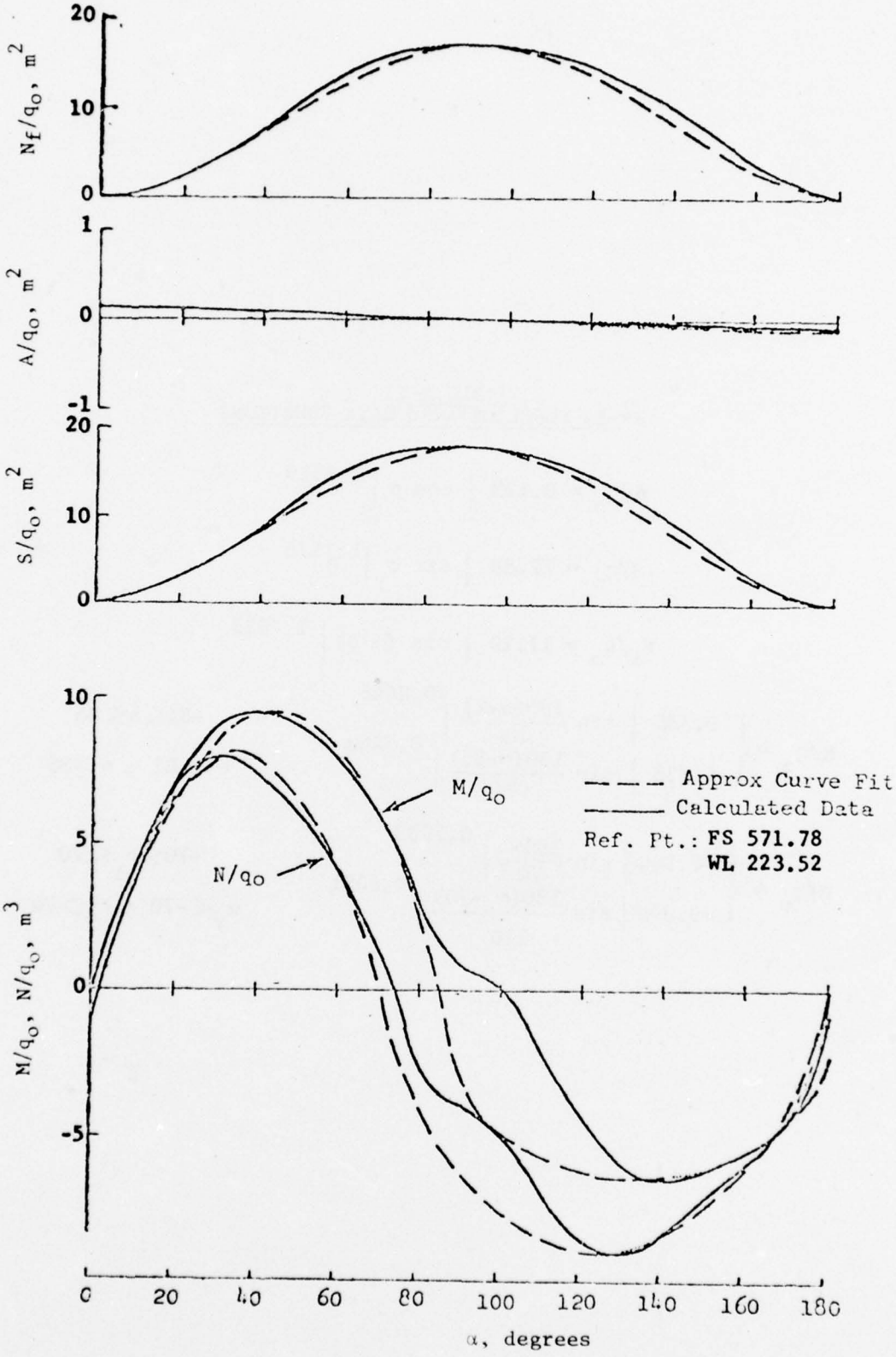

FIGURE A-2: XV-6A FUSELAGE AERODYNAMIC DATA

TABLE A-1I
XV-6A FUSELAGE AERO DATA FUNCTIONS

$$A/q_o = 0.123 \left| \cos \alpha \right|^{1.8519}$$

$$S/q_o = 17.89 \left| \sin \alpha_y \right|^{1.7676}$$

$$N_f/q_o = 17.12 \left| \sin (\alpha-2) \right|^{1.7583}$$

$$M/q_o = \begin{cases} 9.585 \left| \sin \dfrac{180(\alpha-2)}{83} \right|^{0.8046} & -81 \leq \alpha \leq 85 \\ -6.533 \left| \sin \dfrac{180(\alpha-85)}{97} \right|^{0.3468} & \alpha < -81 \ ; \ \alpha > 85 \end{cases}$$

$$N/q_o = \begin{cases} 8.104 \left| \sin \dfrac{180\alpha}{70} y \right|^{0.7983} & -70 \leq \alpha_y \leq 70 \\ -9.099 \left| \sin \dfrac{180(\alpha_y - 70)}{110} \right|^{0.6081} & \alpha_y < -70 \ ; \ \alpha_y > 70 \end{cases}$$

TABLE A-III
WING AND EMPENNAGE AERO DATA

	Wing	Horizontal Stabilizer	Vertical Stabilizer
Reference Area, $S(m^2)$	17.32	4.41	3.32
Aspect Ratio, AR	2.797	4.277	2.730
MAC (m)	2.643	1.180	1.550
Incidence, i(deg)	1.75	0	0
Reference Pt: FS	626.4	1120.1	1079.2
BL	195.6	0	0
WL	280.9	295.4	400.6
Sweep Angle, $\Lambda_{1/4}$ (deg)	34.0	32.9	40.2
Taper Ratio, λ	0.400	0.201	0.230
Body Diameter to Span Ratio, d/b	0.230	0.160	0.163
2-D Lift Curve Slope, a_o (1/deg)	0.106	0.109	0.110
Zero-lift Drag Coefficient, C_{D_o}	0.0073	0.0091	0.0099
Zero-lift Moment Coefficient, C_{m_o}	-0.0065	0	0
Max Lift Coefficient, $(C_{L_{max}})_{W(B)}$	0.870	0.980	1.080
Angle of Attack at Max C_L, $\alpha_{C_{L_{max}}}$ (deg)	23.0	24.3	33.4

Wing Downwash: $\varepsilon/C_{L_W} = 14.07$ deg

Wing Flap Effects: $C_{L_o}/\delta_f = 0.0058$/deg

$\Delta C_{L_{max}}/\delta_f = 0.0026$/deg

$\Delta C_{D_o}/\delta_f = 0.00078$/deg

$C_{m_{\delta_f}} = -0.0005$/deg

Wing Lateral/Directional Characteristics:

$C_{l_{\beta_o}} = 0.060$/rad $\qquad$ $\Delta C_{n_\beta}/C_L^2 = 0.055$/rad

TABLE A-III (Continued)

$\Delta C_{l_\beta}/C_L = -0.130/rad$	$\Delta C_{n_r}/C_L^2 = -0.030/rad$
$\Delta C_{l_r}/C_L = 0.230/rad$	$\Delta C_{n_r}/C_D = -0.420/rad$
$C_{l_p} = -0.211/rad$	$\Delta C_{n_p}/C_L = -0.140/rad$
$C_{n_{\beta_o}} = 0.0$	$\Delta C_{n_p}/C_{D_\alpha} = 18.0$

59,000 newtons maximum installed thrust. The thrust may be vectored from horizontally aft ($\theta_J = 0°$) to five degrees forward of vertical ($\theta_J = 95°$).

Nozzle location and assumed maximum thrust per nozzle are listed in Table A-IV. The Pegasus engine has contra-rotating spools so that its angular momentum is negligible. The maximum inlet mass flow was taken to be 181.45 kg/sec and the resulting ram drag was assumed to act at the centroid of the inlet area (FS 261.2; WL 246.4).

Propulsion induced aerodynamics were approximated using the wind tunnel data of reference (k). The basic data used are shown in Figure A-3 and the functional approximations to these data are given by equations A-1 through A-3 where velocity, V, is assumed to be in knots

$$\Delta L_f/T = -.025 + (.0011944\ V - .00005278\ V^2 + .000000201\ V^3) \sin \theta_J \qquad (A-1)$$

$$\Delta D/T = -.00001386\ V + .000008565\ V^2 \qquad (A-2)$$

$$\Delta M/T = -.15 + (.017082\ V + .00003418\ V^2) \sin \theta_J \qquad (A-3)$$

TABLE A-IV
ENGINE DATA

Nozzle Location	FS (cm)	BL (cm)	WL (cm)	Toe-out (deg)	Max Thrust (N)
Right Forward	465.2	103.8	246.4	5.0	14,768
Left Forward	465.2	-103.8	246.4	5.0	14,768
Right Aft	656.9	79.6	240.4	12.5	14,768
Left Aft	656.9	-79.6	240.4	12.5	14,768

Aircraft control is accomplished by a combination of aerodynamic and reaction controls. The aerodynamic controls consist of conventional ailerons, rudder and stabilizer. The effectiveness and gearing of these surfaces, as modelled, is presented in Figure A-4. Reaction control is achieved by exhausting engine bleed air through nozzles at the aircraft extremities. The locations of these nozzles are shown in Figure A-5. The pitch control

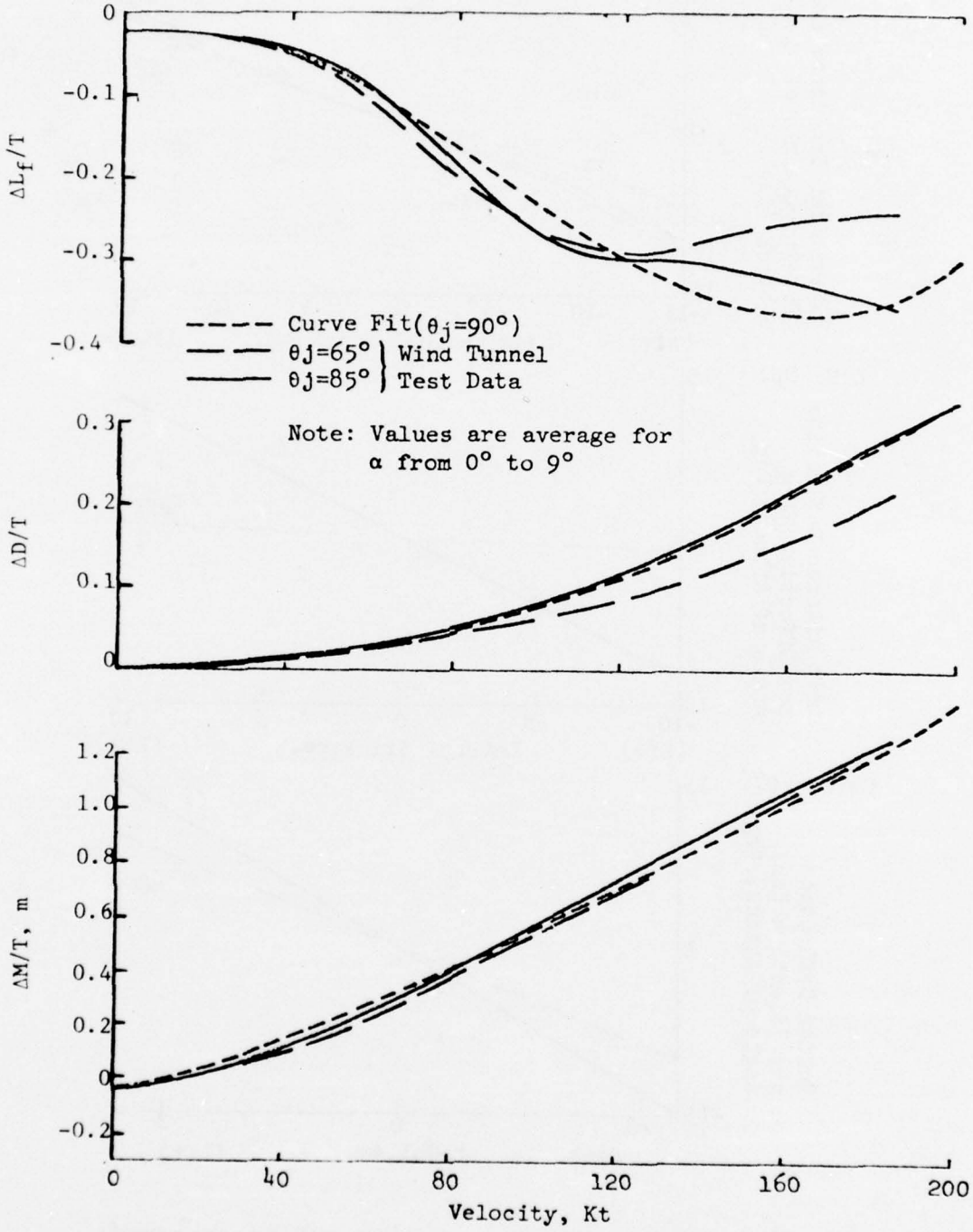

FIGURE A-3: XV-6A PROPULSION INDUCED AERODYNAMICS

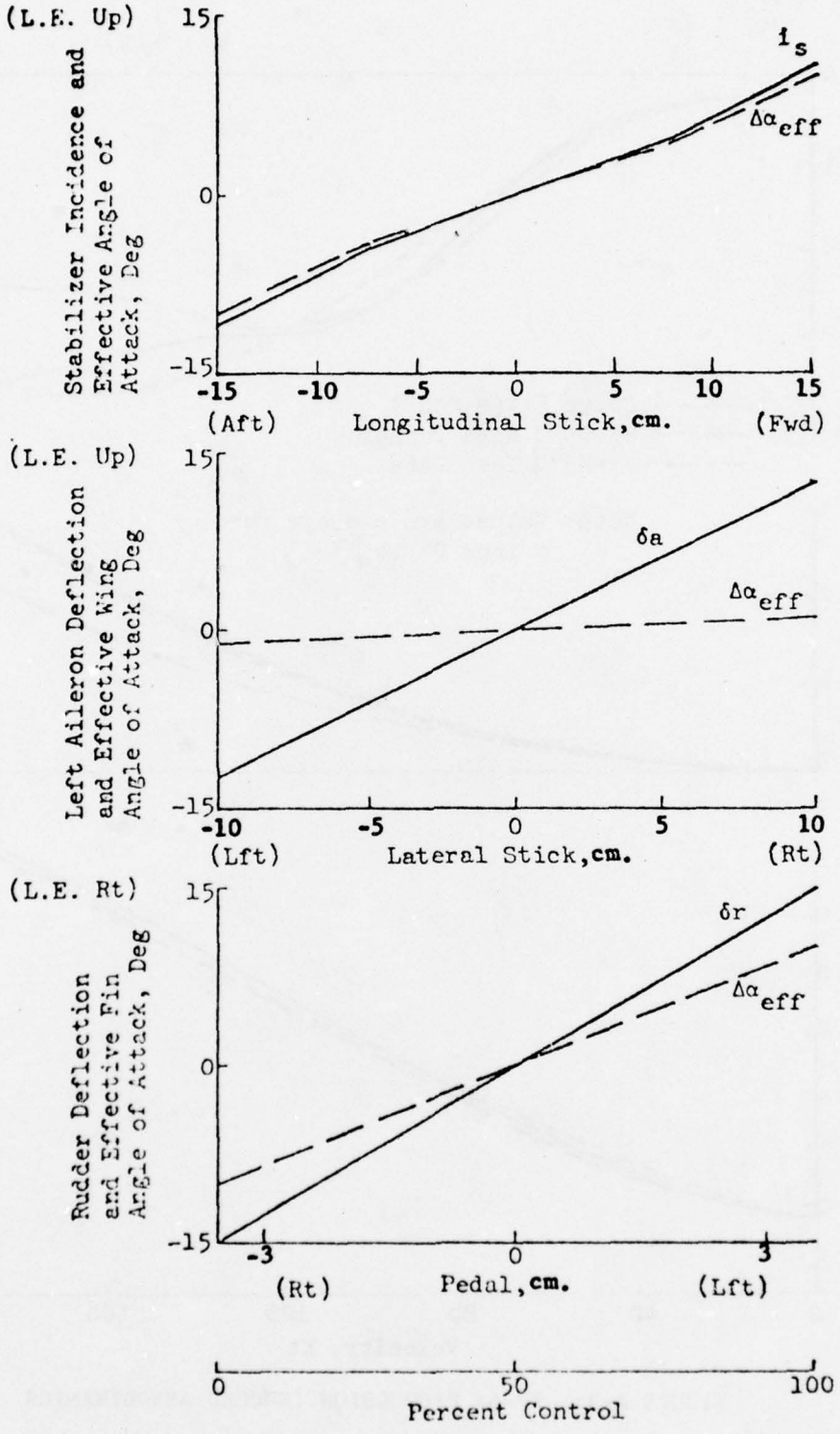

FIGURE A-4: XV-6A AERO CONTROL EFFECTIVENESS AND GEARING

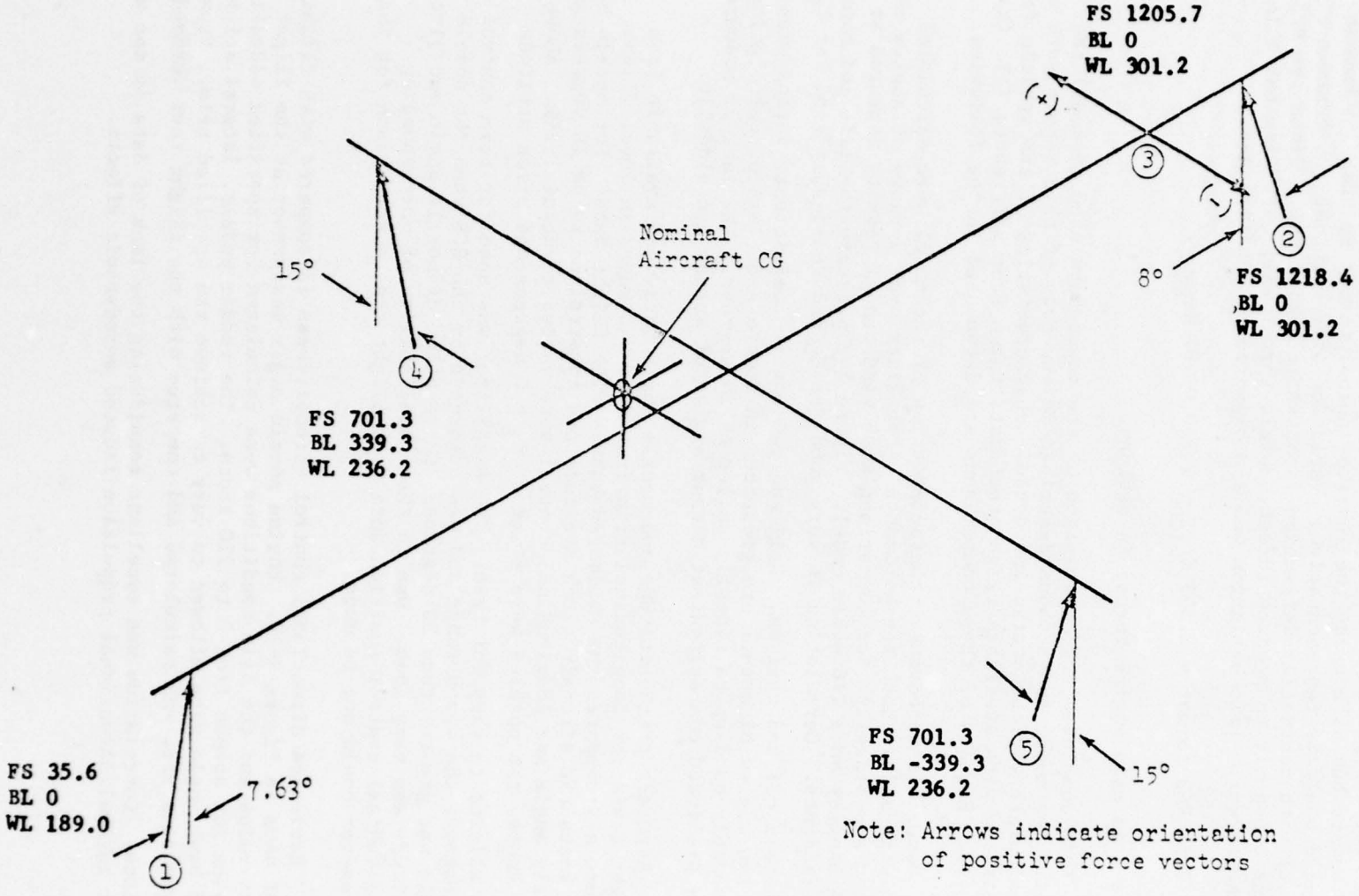

FIGURE A-5: XV-6A RCS NOZZLE LOCATIONS AND ORIENTATIONS

nozzles (1 and 2) thrust only upward, the yaw control nozzle (3) thrusts both left and right and the roll control nozzles (4 and 5) thrust both up and down. For the purposes of this study the roll nozzles were assumed to thrust only upward but with twice the level of actual thrust so that the moment produced would be representative. Variation of RCS thrust (at maximum engine thrust) with controller deflection is shown in Figure A-6. Since the RCS uses engine bleed air to produce thrust, nozzle thrust will vary with the main engine thrust. This variation was approximated by equation A-4.

$$\%\text{max RCS thrust} = 2.393 \left(\frac{T}{1000}\right) - 0.01187 \left(\frac{T}{1000}\right)^2 \qquad \text{(A-4)}$$

where T is main engine thrust in newtons.

This completes the description of the input data used to model the XV-6A. The model and methods described in the body of this report were used to calculate various static and dynamic characteristics of the vehicle for comparison with available flight test data taken from references (j), (k), and (l). Results of these comparisons are documented in the following.

Power off aerodynamic characteristics of the model were calculated both with and without the horizontal stabilizer over a range of angles of attack and sideslips for comparison with wind tunnel results measured at NASA Langley on a 1/6 scale model. Figure A-7 presents the lift and moment coefficients. Correlation is very good for C_L and reasonably good for C_m, both tail off and tail on. Roll and yaw moment coefficients versus sideslip for two angles of attack are presented in Figure A-8. Again, correlation is reasonably good up to sideslip angles of 24 degrees. The lack of measured data precluded comparisons at higher angles of attack and sideslip.

Aircraft pitch attitude and nozzle angle data were available from flight tests for longitudinal trim from 0 to 240 knots in level flight. Figure A-9 compares the estimated values with flight data. For speeds below 140 knots the aircraft pitch attitude was constrained to be 10 degrees and nozzle angle and longitudinal control were varied to obtain trim. Above 140 knots, the nozzles were fixed at $\theta_J = 0$ degrees and pitch attitude was allowed to vary for trim. The stabilizer was used for trim control throughout the speed range and was augmented by the RCS when the nozzle angle was greater than 30 degrees. Correlation of nozzle angle and pitch attitude was very good. Due to the unavailability of corresponding longitudinal control position data from flight test a comparison for this parameter could not be made.

Estimated directional control effectiveness is compared with flight test data in Figure A-10. Engine nozzle angle was preset at the flight test value and the trim conditions were calculated for specified sideslip angles for speeds from 0 to 220 knots. The rudder pedals, lateral stick and bank angle were allowed to vary to achieve the specified trim. From these data β/δ_r was calculated and compared with the flight test derived values. Correlation was excellent considering the lack of data in the model for lateral/directional propulsion induced aerodynamic effects.

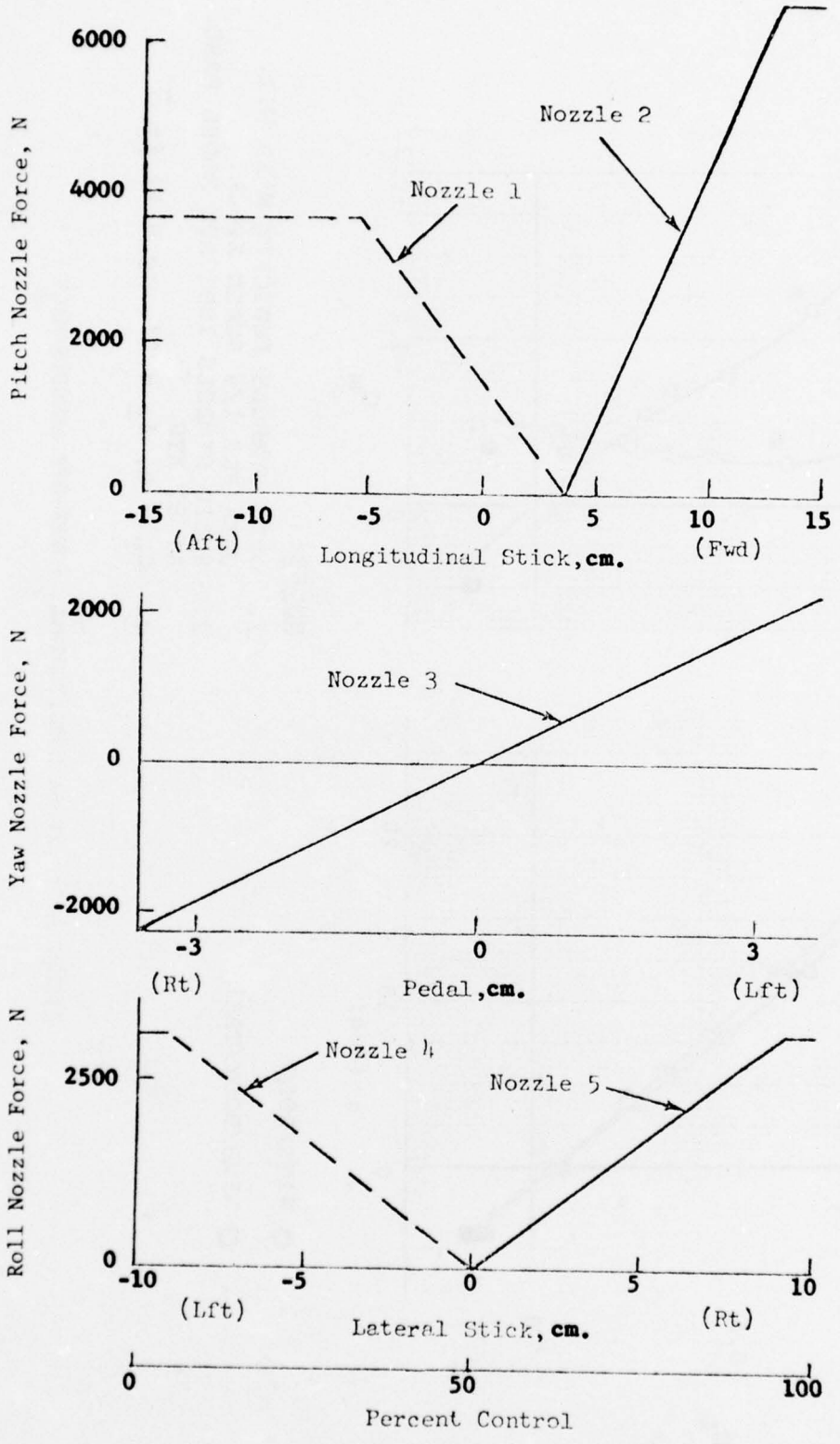

FIGURE A-6: XV-6A RCS THRUST CONTROL

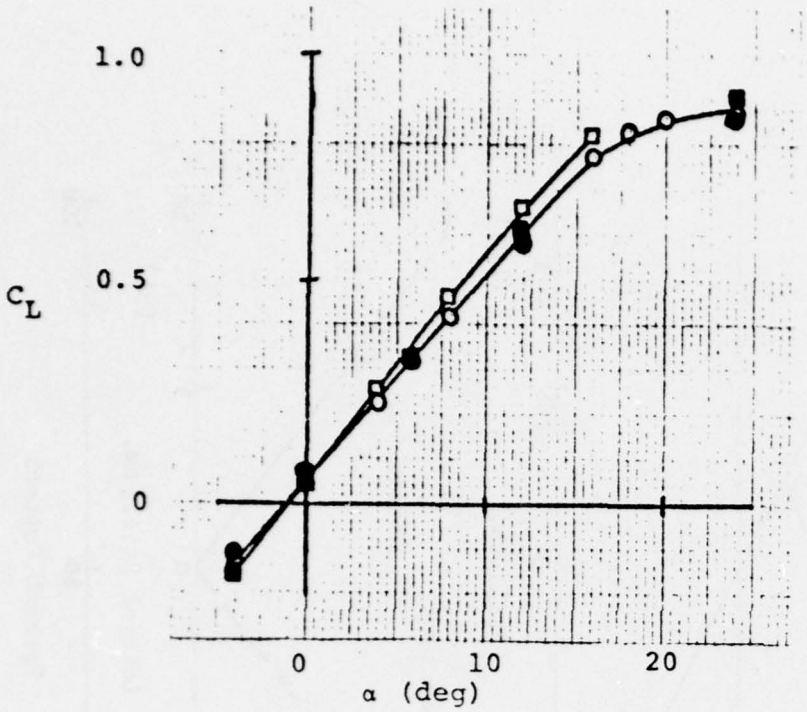

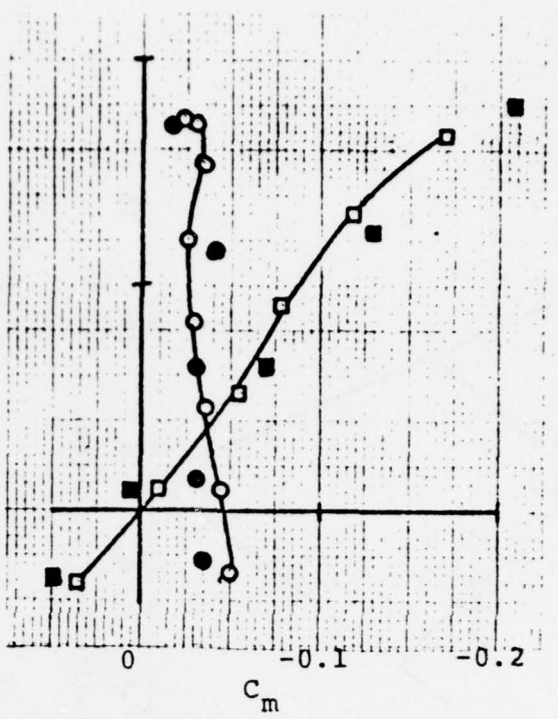

○ WING/BODY

□ WING/BODY/TAIL

NOTES:

1. OPEN SYMBOLS INDICATE NASA W.T. DATA FOR 1/6 SCALE XV-6A.
2. SOLID SYMBOLS INDICATE MODEL PRED. AT 57 KTS.
3. $C_T = 0$, $\delta_f = 0°$, cg @ 12.8% $\bar{c}$

FIGURE A-7: XV-6A LONGITUDINAL, POWER-OFF AERODYNAMICS

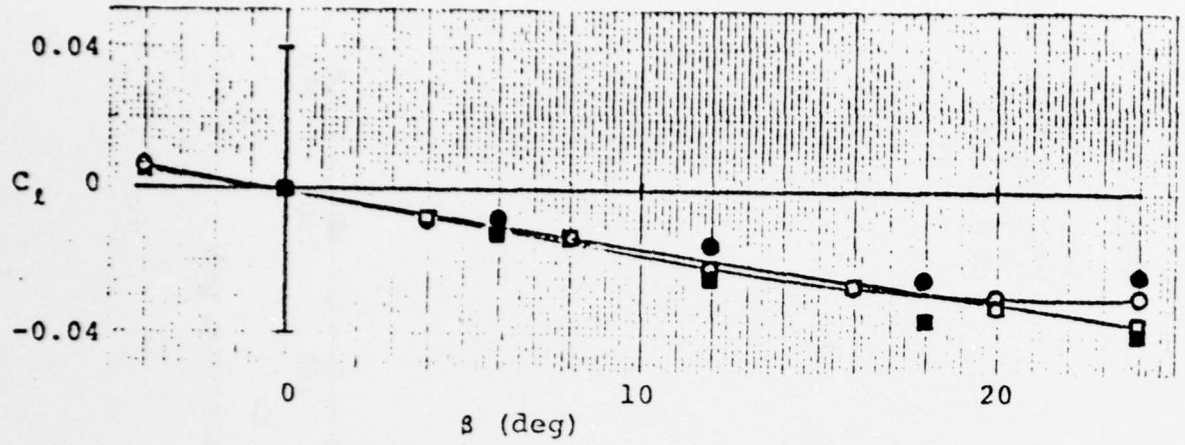

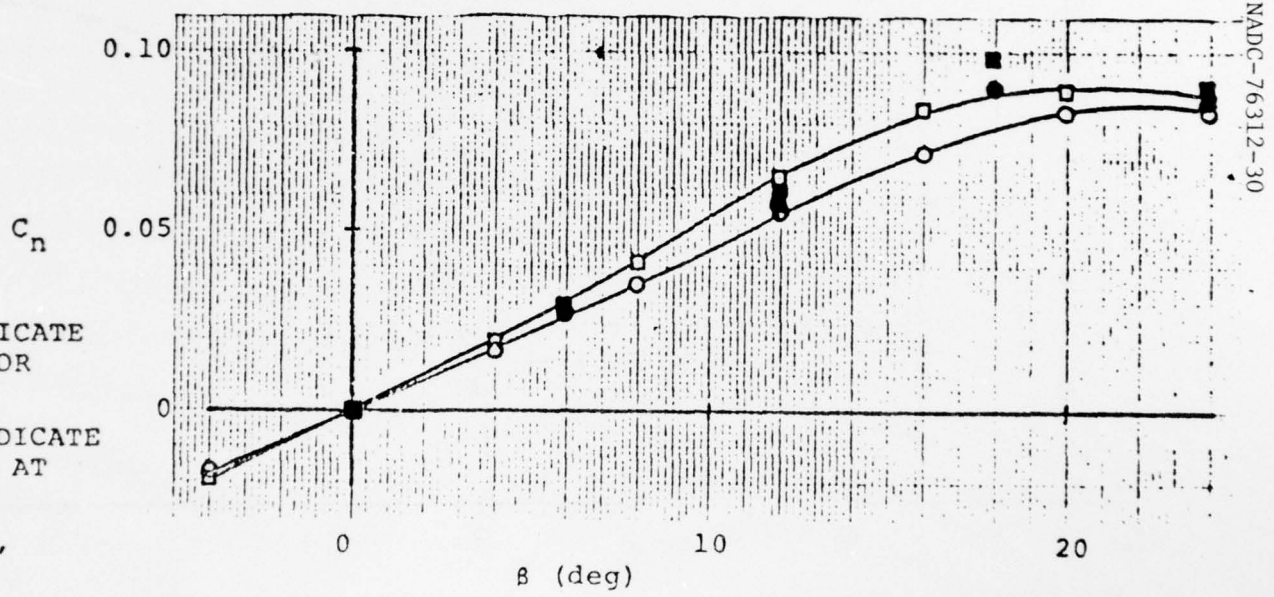

NOTES:

1. OPEN SYMBOLS INDICATE NASA W.T. DATA FOR 1/6 SCALE XV-6A.
2. SOLID SYMBOLS INDICATE MODEL PREDICTION AT 57 KTS.
3. $C_T = 0$, $\delta_f = 60°$, cg @ 12.8% $\bar{c}$

NADC-76312-30

FIGURE A-8: XV-6A LATERAL/DIRECTIONAL, POWER-OFF AERODYNAMICS

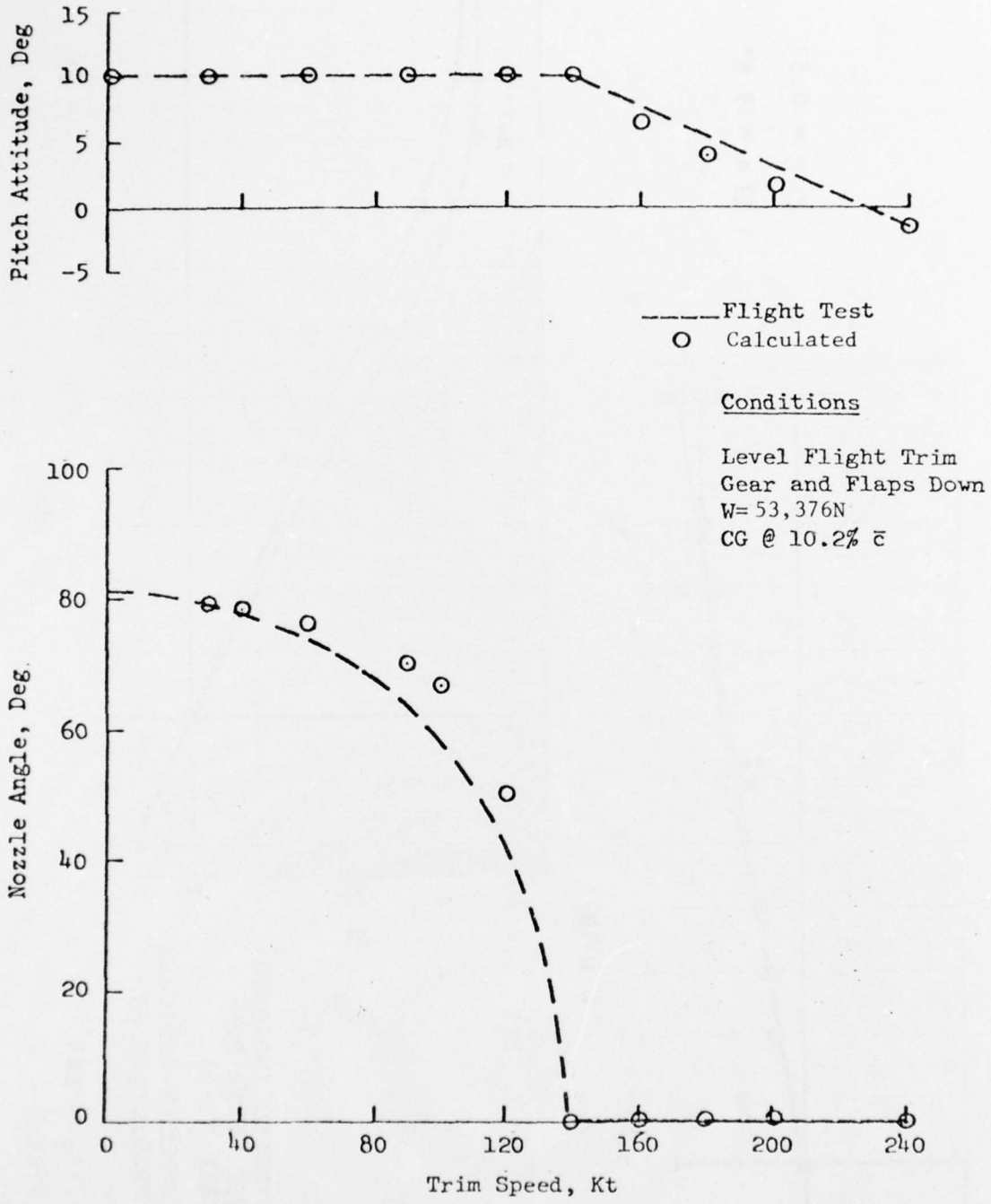

FIGURE A-9: XV-6A LONGITUDINAL TRIM

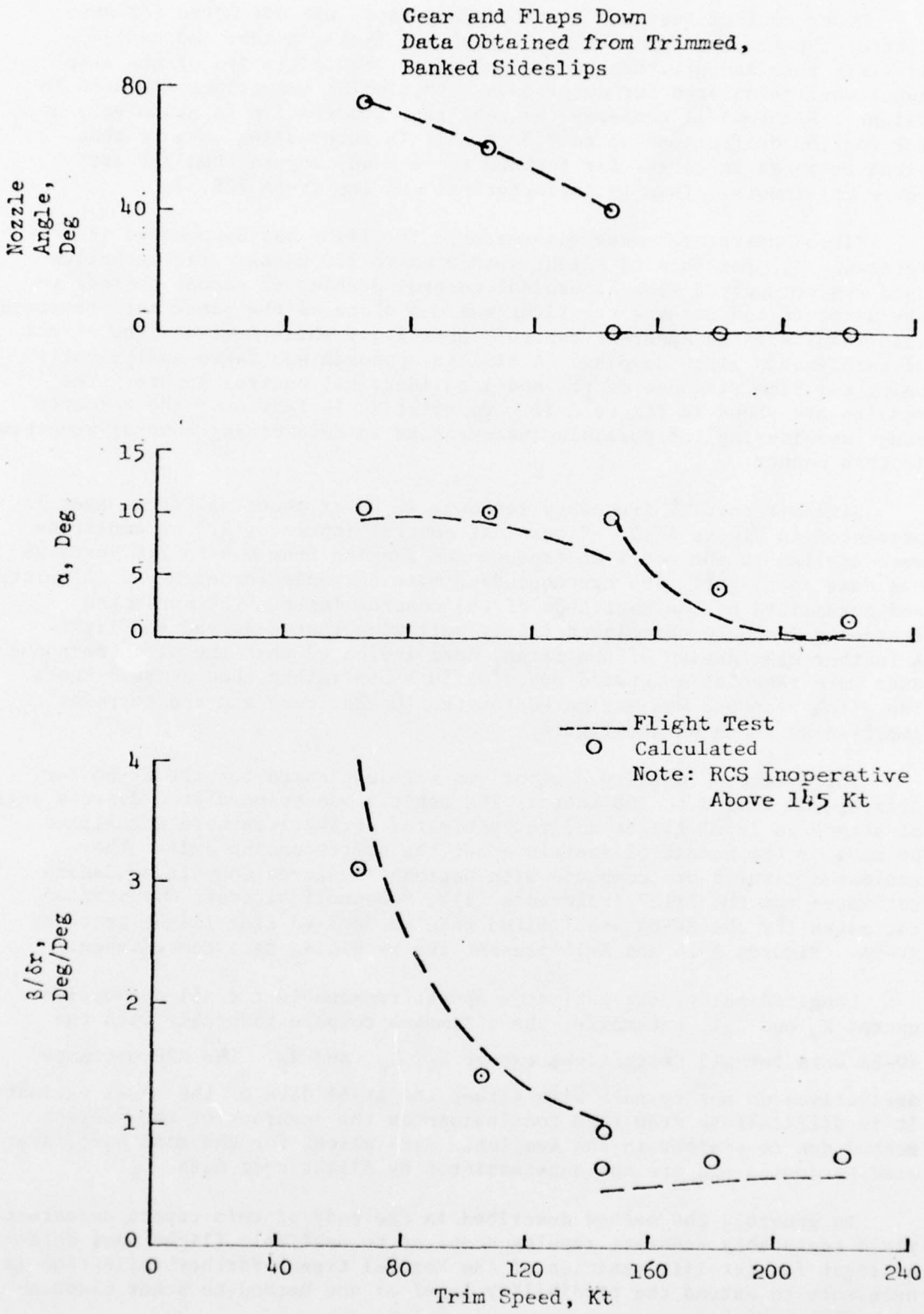

FIGURE A-10: XV-6A DIRECTIONAL CONTROL EFFECTIVENESS

Hover control response (attitude and rate) was estimated for step control inputs about each of the three axes (roll, pitch, and yaw). Aircraft rate and attitude one second after the initiation of the step input were calculated for comparison with similar quantities measured in flight. Figure A-11 compares the results. Correlation is again very good for control deflections up to 2.5 cm. It is interesting to note that pitch response is larger for forward (nose down) inputs than for aft (nose up) inputs. This is characteristic of the XV-6A RCS.

Pitch control response was measured in flight and documented in reference (j) for forward flight speeds up to 220 knots. The technique used was to apply a slow sinusoidal control doublet (2 second period) to the aircraft and measure the first maximum slope of the pitch rate response. This results in an apparent control sensitivity which includes the effect of aerodynamic pitch damping. A similar approach was taken analytically using the time response of the model to identical control inputs. The results are shown in Figure A-12. Correlation is fair over the velocity range considering the possible inaccuracies in determining control sensitivity in this manner.

Aircraft angular frequency response in hover about all three axes is presented in Figure A-13. Sinusoidal control inputs of 2.5 cm amplitude were applied to the model at frequencies ranging from 0.4 to 2.0 Hertz as was done in flight. The corresponding rate response for each was calculated and normalized by the amplitude of the control input. The estimated frequency response correlated fairly well with that measured in flight. A further examination of the flight data indicated that the pitch response data were taken at a forward speed of 10 knots rather than at zero knots. The pitch response was estimated for the 10 knot case and the correlation improved as shown on the figure.

The primary stability derivatives were estimated for the XV-6A for trim speeds from 0 to 100 knots. The vehicle was trimmed at 8 degrees angle of attack in level flight and the estimated derivatives were normalized by mass or the moment of inertia about the corresponding axis. The estimated results are compared with National Research Council of Canada estimates for the P1127 (reference (1)), McDonnell Aircraft Corporation estimates for the AV-8A and limited results derived from flight tests of XV-6A. Figures A-14 and A-15 present the resulting data comparisons.

Longitudinally, the estimates appear reasonable for all derivatives except X_w and Z_u. Laterally, the estimates compare favorably with the AV-8A data for all derivatives except L_v, L_r, and N_p. The NRC estimated derivatives do not compare with either the AV-8A data or the model estimates. It is difficult to draw firm conclusions on the accuracy of the subject method due to scatter in the available data which, for the most part, are also estimates and are not substantiated by flight test data.

In general, the method described in the body of this report appears to yield reasonably accurate results compared to available flight test data--at least for jet-lift vehicles of the Kestrel type. Further validation is necessary to extend the credibility level of the method to other classes of V/STOL vehicles.

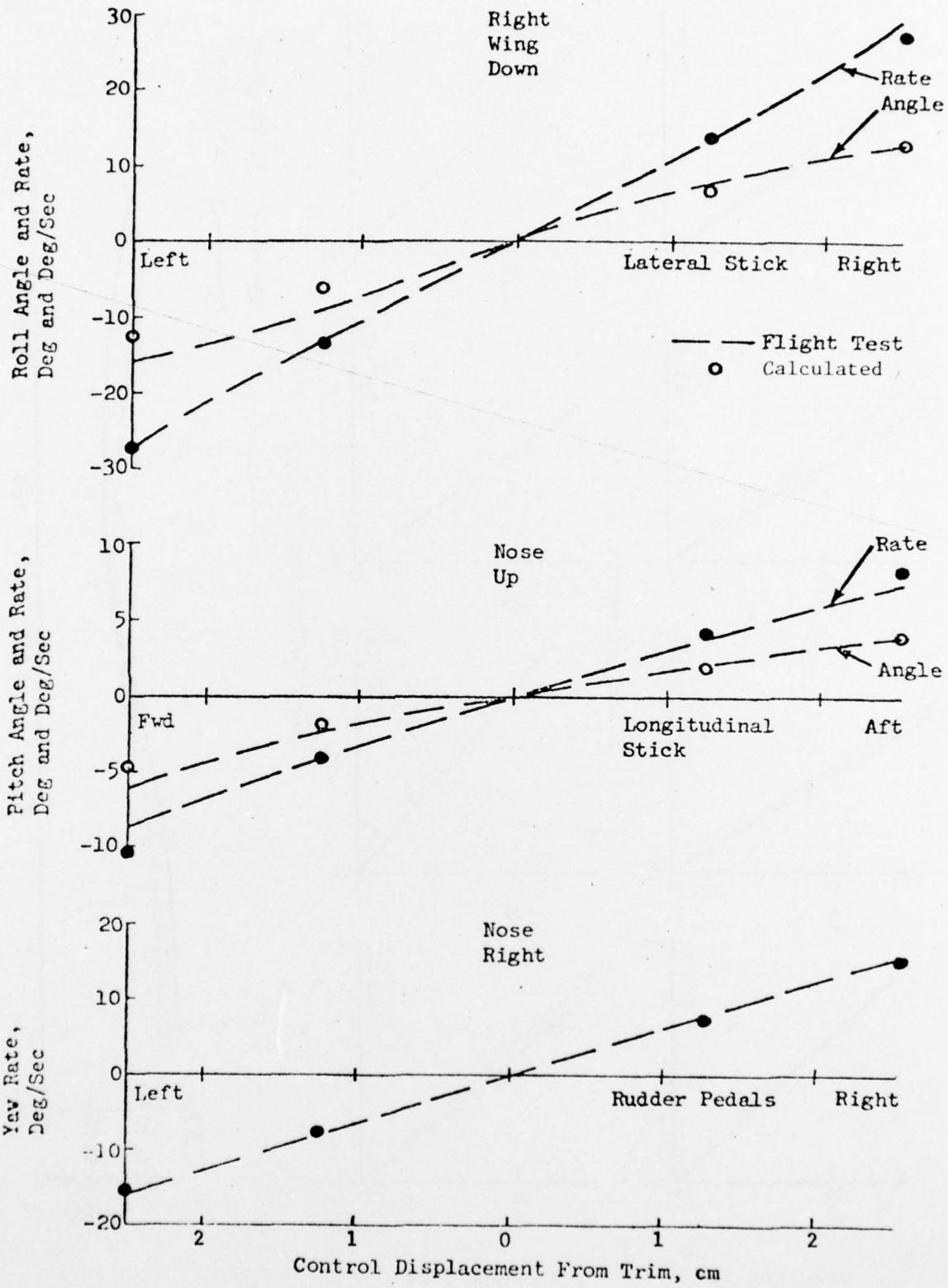

FIGURE A-11: XV-6A HOVER CONTROL RESPONSE

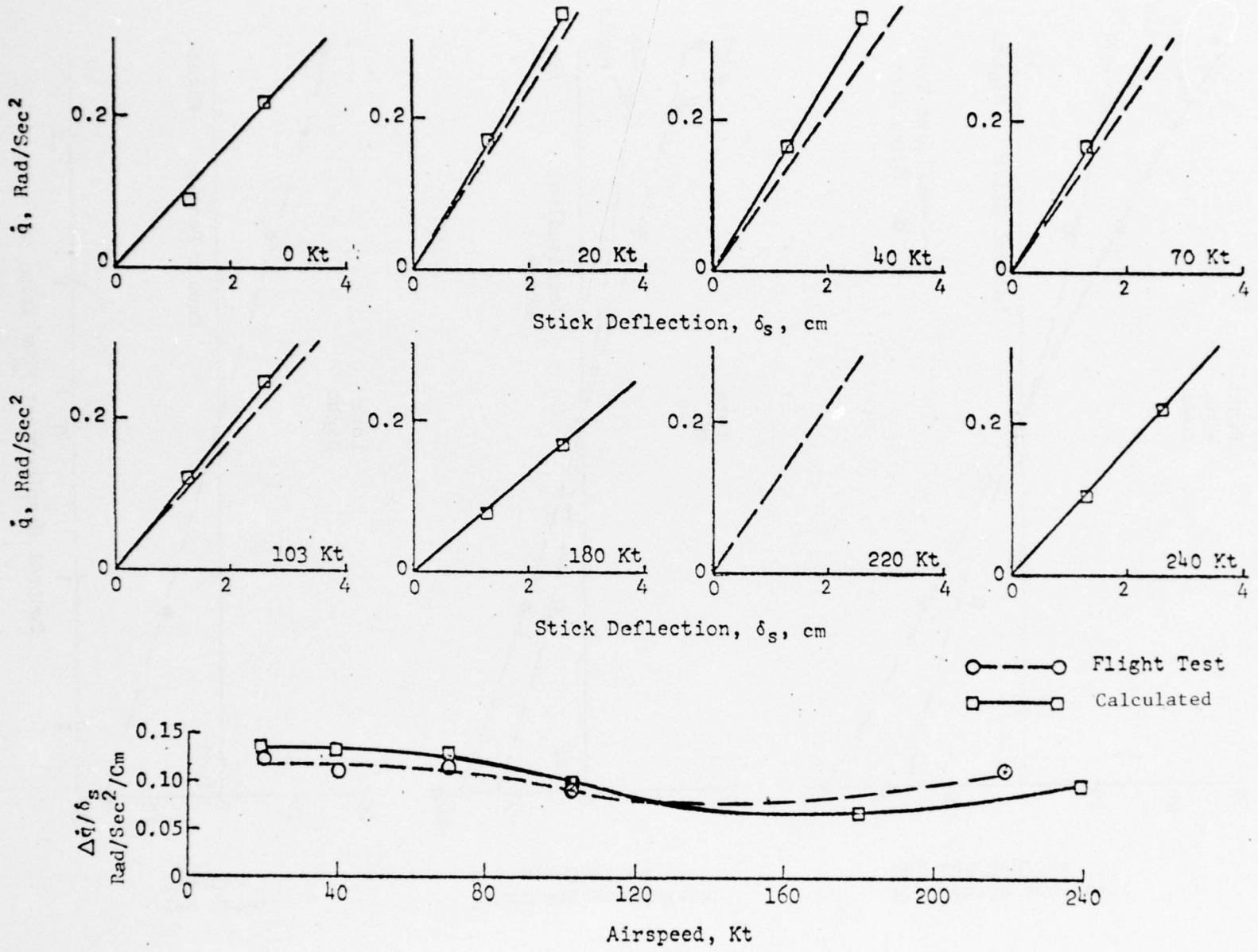

FIGURE A-12: XV-6A PITCH CONTROL SENSITIVITY

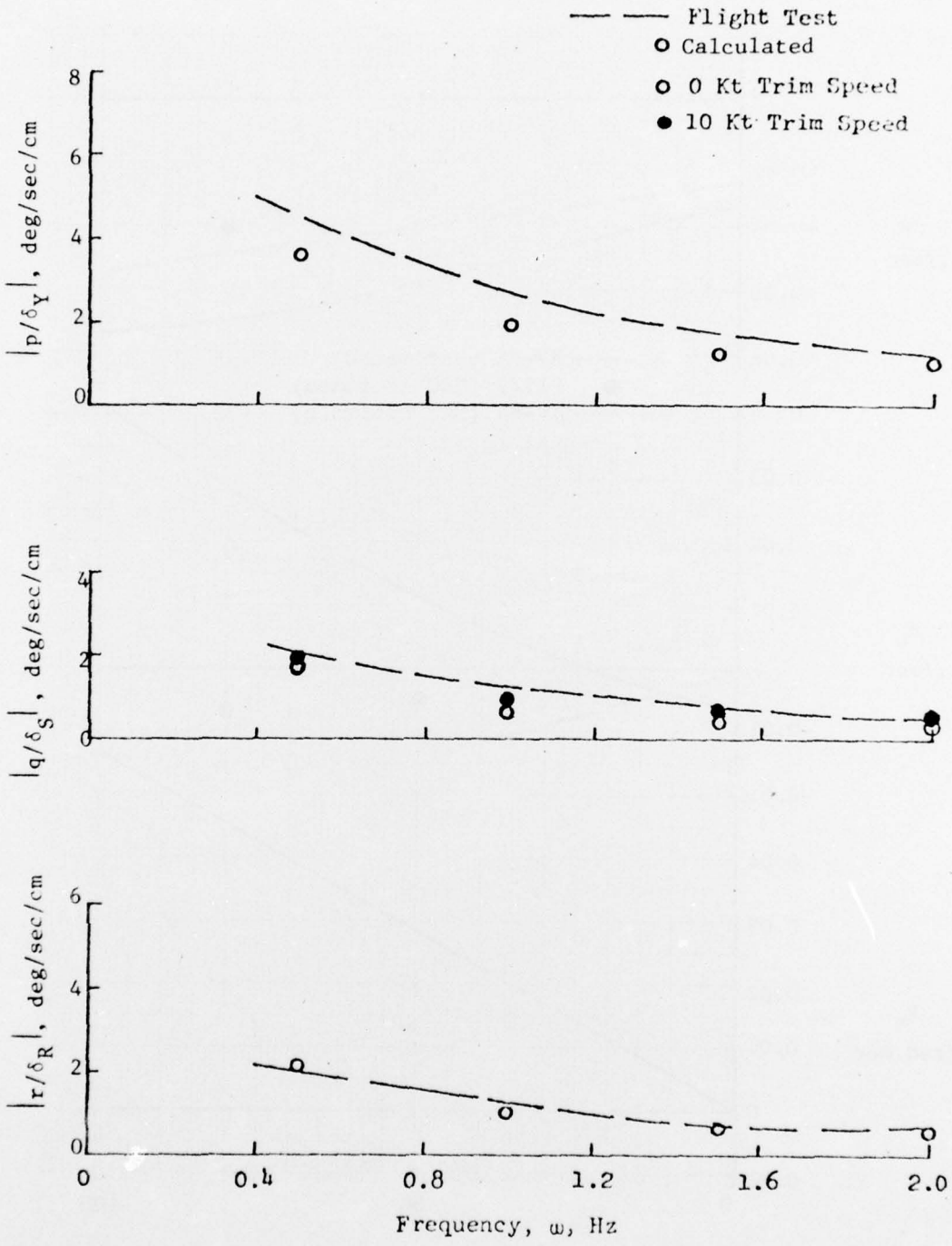

FIGURE A-13: XV-6A FREQUENCY RESPONSE IN HOVER

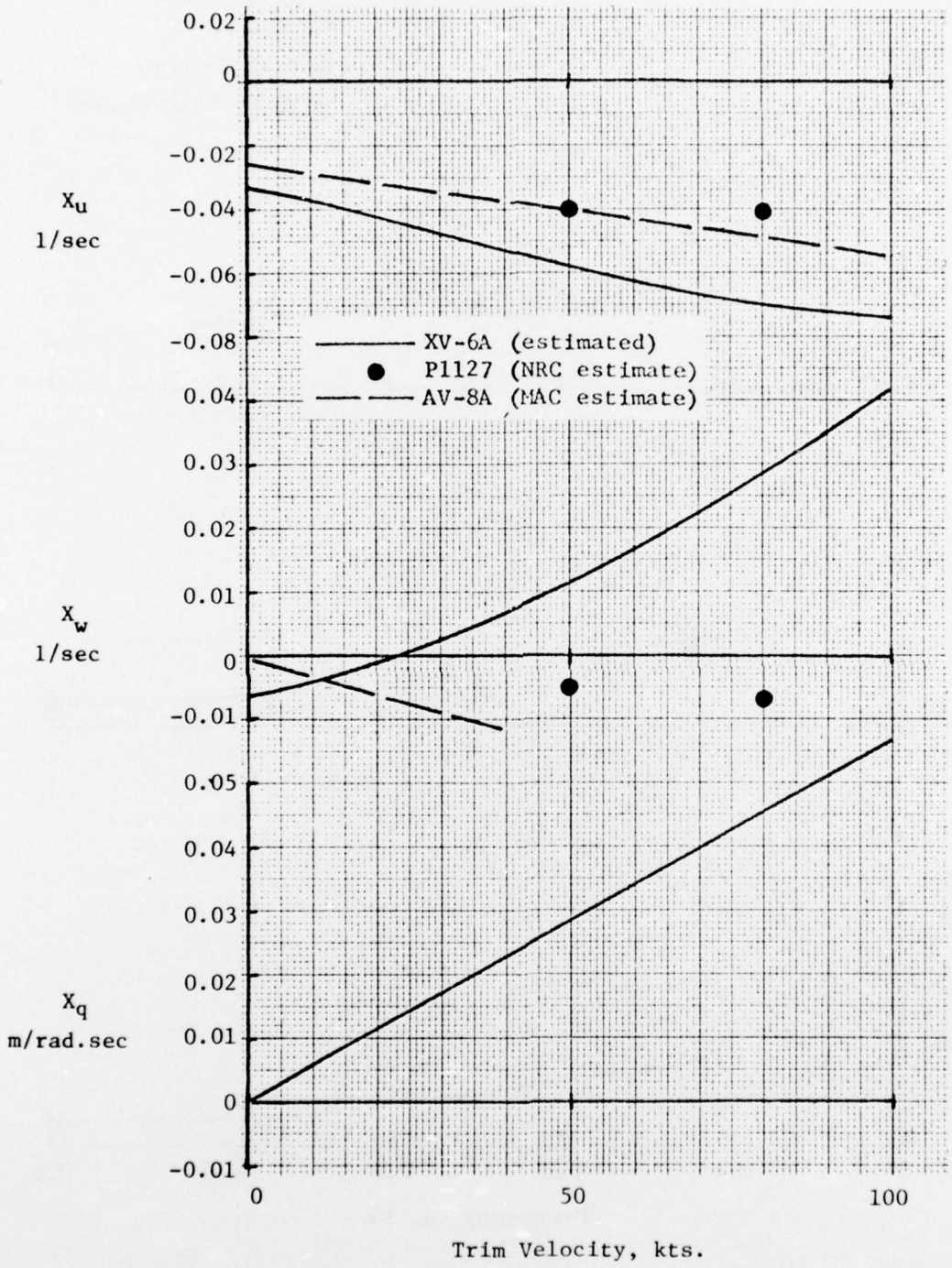

FIGURE A-14 (a): XV-6A LONGITUDINAL STABILITY DERIVATIVES

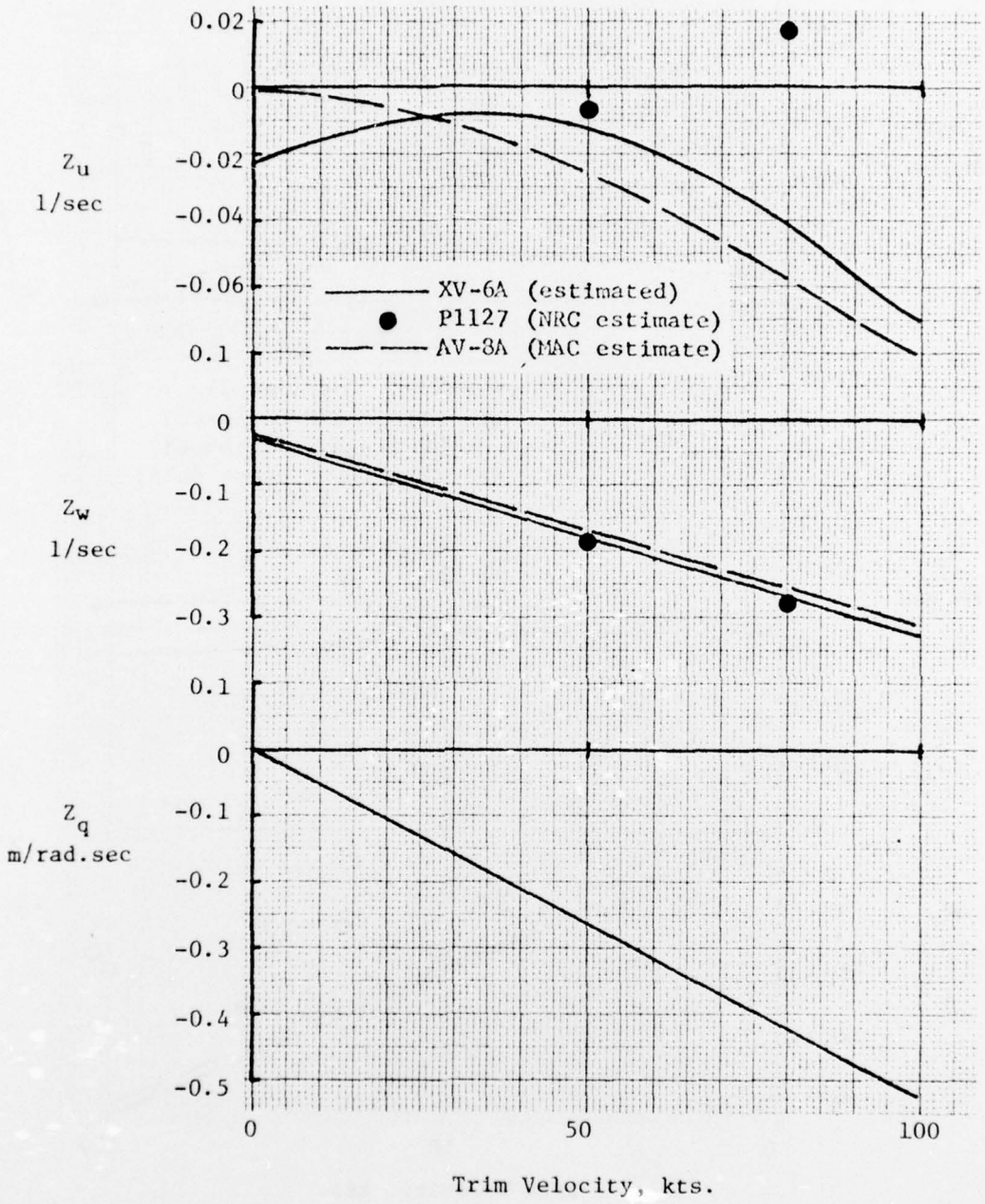

FIGURE A-14 (b): XV-6A LONGITUDINAL STABILITY DERIVATIVES (con'd)

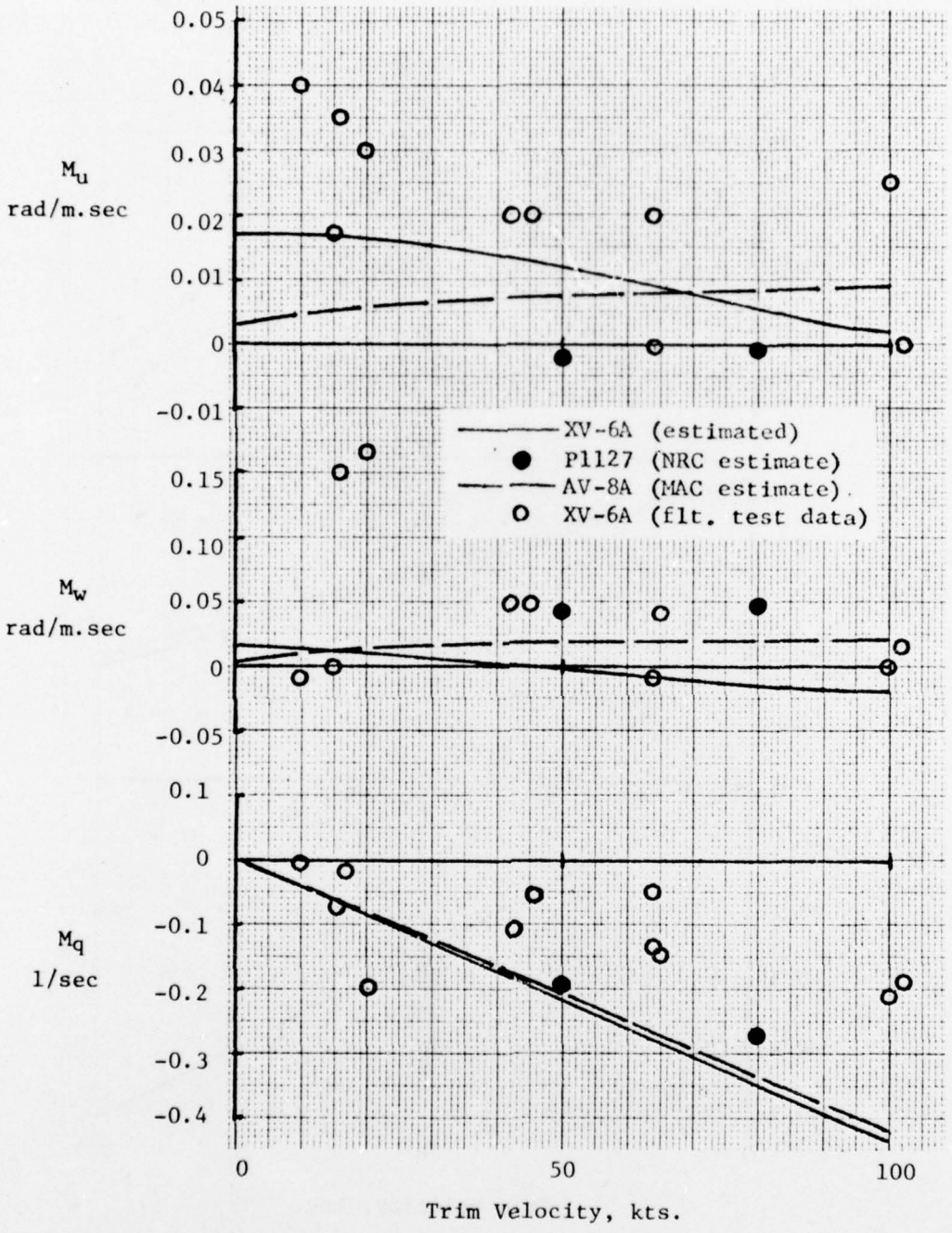

FIGURE A-14 (c): XV-6A LONGITUDINAL STABILITY DERIVATIVES (con'd)

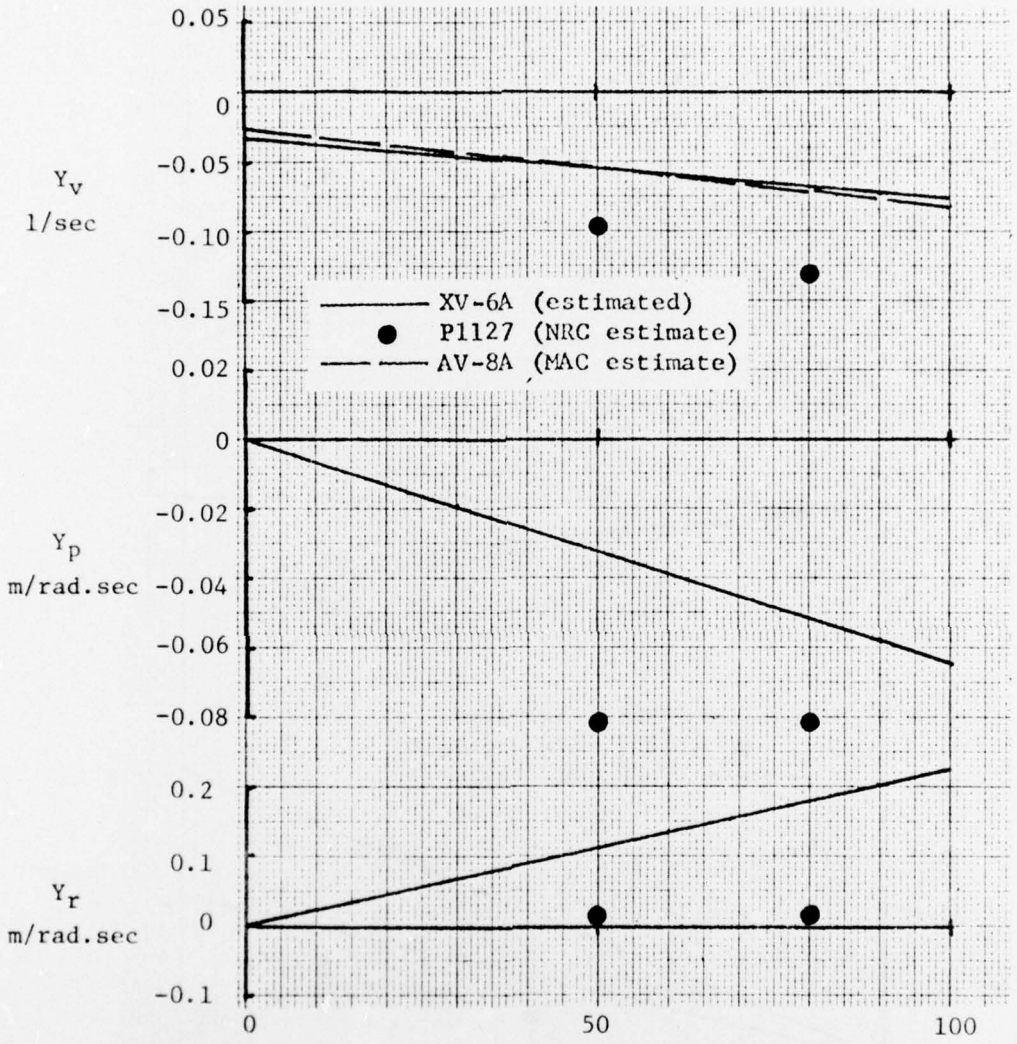

FIGURE A-15 (a): XV-6A LATERAL/DIRECTIONAL STABILITY DERIVATIVES

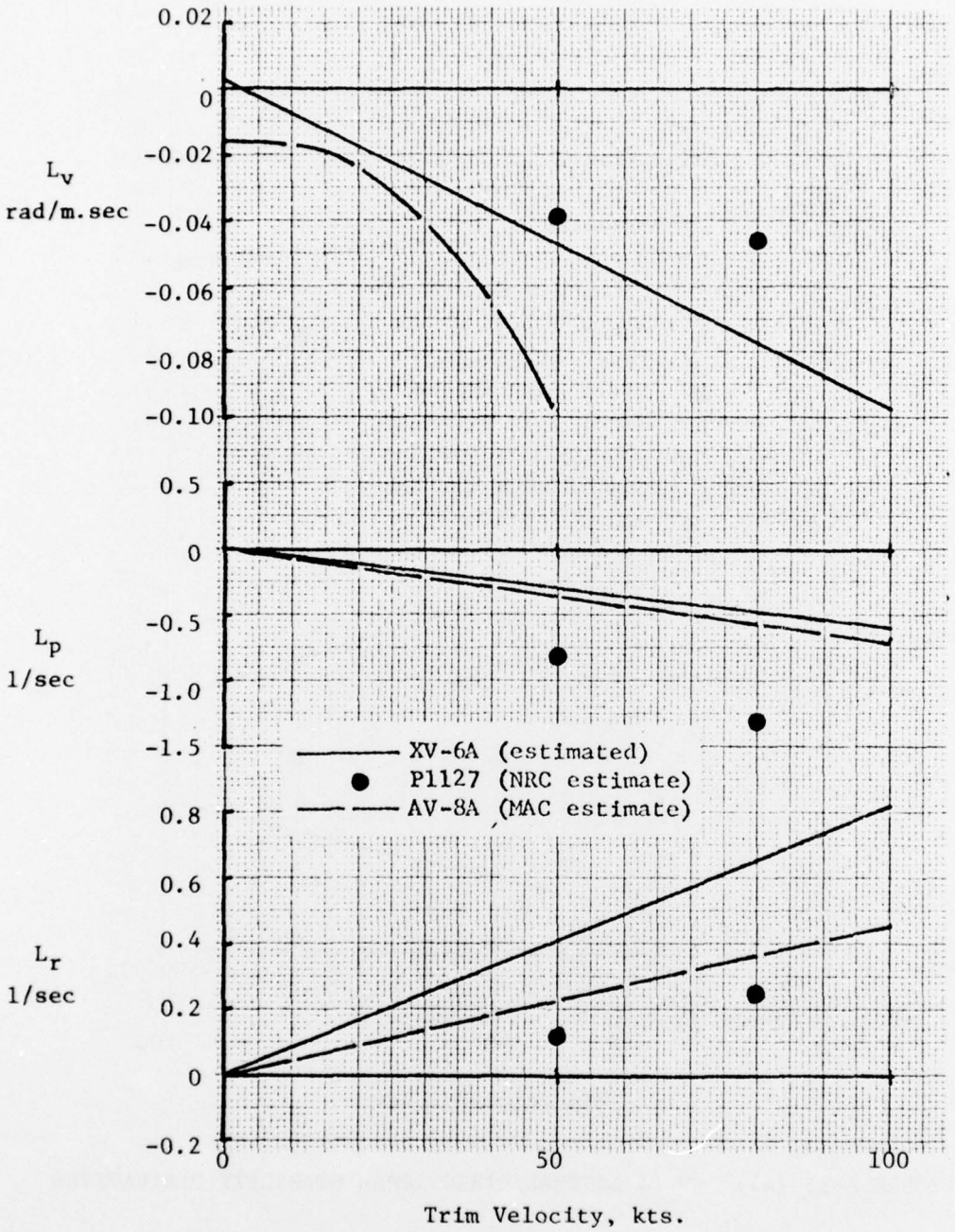

FIGURE A-15 (b): XV-6A LATERAL/DIRECTIONAL STABILITY DERIVATIVES (con'd)

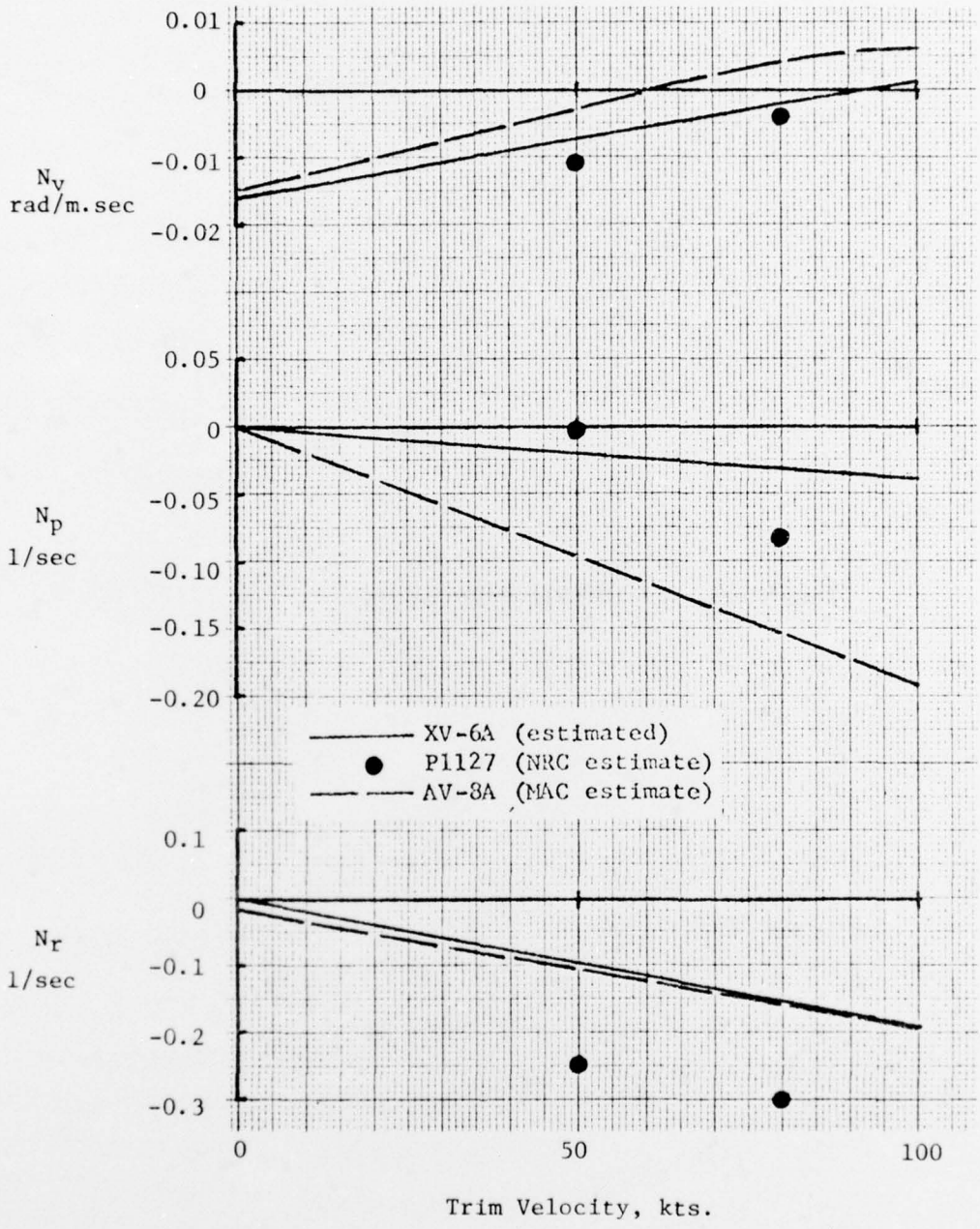

FIGURE A-15 (c): XV-6A LATERAL/DIRECTIONAL STABILITY DERIVATIVES (con'd)

DISTRIBUTION LIST

REPORT NO. NADC-76312-30

AIRTASK NO. A03V-320D/001B/6F41421201

	No. of Copies
NAVAIRSYSCOM (AIR-954) (2 for retention) (2 for AIR-320D) (1 for AIR-5301)	5
DDC	12
NASA, Ames Research Center (1 for S. Anderson)	1
NASA, Langley Research Center (1 for R. Margason)	1
NAVSHIPRSCHDEVCEN (1 for 166)	1
NAVWPNCEN	1
Office of Naval Research (1 for D. Siegel)	1
Naval Postgraduate School (1 for L. Schmidt)	1
AFFDL (ASD/ENFDH), WPAFB, OH	1
Army Aviation Systems Command, St. Louis, MO	1
General Dynamics, CAD, San Diego, CA	1
The Boeing Company, Seattle, WA (1 for H. Higgins)	1
LTV Aerospace Corporation, Dallas, TX (1 for W. Straub)	1
Rockwell International, Columbus, OH	1
McDonnell Douglas Corporation, St. Louis, MO	1
Northrup Corp., Hawthorne, CA (1 for W. Martin)	1
Grumman Aerospace Corporation, Bethpage, NY	1
Boeing Vertol, Philadelphia, PA (1 for H. Rosenstein)	1